MOLECULAR DYNAMICS STUDIES ON WETTING BEHAVIOR OF SILICON SURFACES AND HEAT TRANSFER CHARACTERISTICS OF ELECTROLYTE SOLUTION FILLED SILICON NANO-CHANNELS

A Thesis Submitted to
the Graduate School of Engineering and Science of
İzmir Institute of Technology
in Partial Fulfillment of the Requirements for the Degree of

MASTER OF SCIENCE

in Mechanical Engineering

by
Abdullah Cihan ÖZDEMİR

July 2020
İZMİR

ACKNOWLEDGMENTS

I would like to express my sincere gratitude to my advisor Assoc. Prof. Dr. Murat BARIŞIK for his patience, support, guidance, encouragement, and suggestions. I have been grateful that he has always shared his background, vision, academic knowledge, and experience with me since I started studying for a master's degree.

I also would like to thank Prof. Dr. Ali BEŞKÖK and Center for Scientific Computation at Southern Methodist University.

During my thesis, I was happy to be part of the MinaEng (Micro/Nano Engineering Group of Izmir Institute of Technology), and I would like to thank all of the group members for their friendship and information sharing, especially to H. Gökberk ÖZÇELİK, Safa SABET and B. Öykü ALAN.

This work was supported by the Scientific and Technological Research Council of Turkey (TÜBİTAK) under the Grant Number 217M460. I also thank for the support from the Turkish Academy of Sciences (TUBA) in the framework of the Young Scientist Award Programme (GEBIP).

Last but not the least, I am thankful to my family for endless care, love, and encouragement. They also support me every time during my educational life.

ABSTRACT

MOLECULAR DYNAMICS STUDIES ON WETTING BEHAVIOR OF SILICON SURFACES AND HEAT TRANSFER CHARACTERISTICS OF ELECTROLYTE SOLUTION FILLED SILICON NANO-CHANNELS

Silicon has always been of interest to researchers from various fields, especially the semiconductor industry. Silicon and silicon-based materials are frequently used in integrated circuits and micro/nano-electro-mechanical systems. Interfacial phenomena between phases is important for these applications. In this study, surface wetting and heat transfer at the solid/liquid interfacial region were investigated using the Molecular Dynamics method. The control of wetting was examined by changing silicon structure at single crystal and amorphous forms and was correlated with the surface coating thickness. Contact angles on both single crystal and amorphous surfaces were calculated. To understand the molecular regions affecting the contact angle, the near interface height parameter was defined as the distance from the surface. Then, interface densities and contact angles of single crystal and amorphous structures were calculated at each height parameter. We defined an effective range of intermolecular forces for the control of wetting. Second, heat transfer characteristics at water/silicon interfaces were examined. Solid/liquid interface is important to determine heat transfer at nanoscale. We focused on the influence of ionic conditions on heat transfer for a water-NaCl solution between two silicon walls. The surface charge density showed variation by ionic condition. We calculated surface charges naturally forming at the corresponding electrolyte concentration. With the increase in salinity, the electrolyte solution density increased and thermal conductivity decreased. Results showed good agreement with the experimental measurements. Additionally, we observed a 35% increase in heat transfer due to a decrease in interfacial thermal resistance by increasing ionic concentration to the highest salinity value of standard conditions. Heat transfer at solid/liquid interface characterized by Kapitza length was correlated with the salinity.

Keywords: Solid/Liquid Interfacial Phenomena, Wetting, Nanoscale Heat Transfer, Molecular Dynamics

ÖZET

SİLİKON YÜZEYLERİN ISLATMA DAVRANIŞLARI VE ELEKTROLİT ÇÖZELTİSİ DOLU SİLİKON NANO-KANALLARIN ISI TRANSFER ÖZELLİKLERİ ÜZERİNE MOLEKÜLER DİNAMİK ÇALIŞMALARI

Silikon, özellikle yarı iletken endüstrisi başta olmak üzere çeşitli alanlardaki araştırmacıların ilgisini çekmiştir. Silikon ve silikon bazlı malzemeler, entegre devrelerde ve mikro/nano-elektro-mekanik sistemlerde sıklıkla kullanılır. Fazlar arasındaki arayüzey olayları bu uygulamalar için önemlidir. Bu çalışmada katı/sıvı arayüzey bölgesindeki yüzey ıslatma ve ısı transferi Moleküler Dinamik yöntemi kullanılarak araştırılmıştır. Islatmanın kontrolü, farklı silikon tek taneli ve amorf yüzeyler kullanılarak incelenmiş ve yüzey kaplama kalınlığı ile ilişkilendirilmiştir. Hem tek taneli hem de amorf yüzeylerin su damlacıkları ile yaptığı temas açısı ölçülmüştür. Temas açısını etkileyen moleküler bölgeleri anlamak için, arayüz yükseklik parametresi yüzeyden uzaklık olarak tanımlandı. Daha sonra, her yükseklik parametresinde tek taneli ve amorf yapıların arayüz yoğunlukları ve temas açıları hesaplandı. Islanmanın kontrolü için etkili bir moleküller arası kuvvet aralığı tanımladık. İkinci olarak, su/silikon arayüzlerinde ısı transfer karakteristikleri incelendi. Nano boyutlarda ısı transferini belirlemek için katı/sıvı arayüz özellikleri önemlidir. İki silikon duvar arasına doldurulan su-NaCl çözeltisi için iyonik koşulların ısı transferi üzerindeki etkisine odaklandık. Yüzey yük yoğunluğu iyonik koşullara göre değişiklik gösterdiğinden, karşılık gelen elektrolit konsantrasyonunda doğal olarak oluşan yüzey yüklerini hesapladık. Tuzluluk artışı ile elektrolit çözeltisi yoğunluğu artmış ve termal iletkenlik azalmış olup sonuçlar ise deneysel ölçümlerle iyi uyum göstermiştir. Ayrıca, artan iyonik konsantrasyonu ile arayüzey ısıl direncinin azalması nedeniyle ısı transferinde % 35 artış gözlemledik. Katı/sıvı ara yüzeyindeki ısı transferi, tuzluluk değişimiyle ile ilişkilendirilen Kapitza uzunluğu ile karakterize edilmiştir.

Anahtar Kelimeler: Katı/Sıvı Arayüz Olayları, Islanma, Nano Boyutta Isı Transferi, Moleküler Dinamik

TABLE OF CONTENTS

LIST OF FIGURES

Figure **Page**

Figure **Page**

LIST OF TABLES

Table **Page**

LIST OF SYMBOLS

r_b	Base radius	nm
r	Distance of molecules	nm
q	Electrostatic charge, heat flux	e, W/m^2
a	Acceleration	m/s^2
h	Height parameter	nm
C	Concentration of NaCl	M
Q_C	Electron charge	C
A	Surface area	nm^2
pH	pH level	
$\#_{counterions}$	Number of counterions	
$\#_{co-ions}$	Number of co-ions	
N	Number of molecules	
$\partial T/\partial z$	Temperature gradient	K/nm
k	Thermal conductivity	W/mK
L_k	Kapitza length	nm

Greek Letters

ɣ	Interfacial tension	N/m
θ	Contact angle	degree
τ	Line tension	N
ΔT	Temperature jump	K
λ	Debye length	nm
ε	Interaction strength, dielectric constant	eV, F/m
σ	Molecular diameter	nm
Δt	Time step	ps
σ_s	Surface charge density	C/m^2
ρ	Density	g/cm^3

Subscripts

B	Base
S	Solid
L	Liquid
V	Vapor
s	Surface
C	Charge
k	Kapitza

CHAPTER 1

INTRODUCTION

The study of materials at the atomic, molecular level between 1-100 nm dimensions is called nanoscience, and the design, characterization, modeling, and production of these dimensions are called nanotechnology and nanotechnology is a science that requires interdisciplinary study of chemistry, photonics, materials, and engineering. With the development of technology and production methods, the need for nanoscale engineering studies has increased. Nanoscale studies that can be seen in various disciplines of engineering, chemical engineering; in catalysts[1], surface science in catalysis[2], electric-electronic engineering; in nanophotonic[3], civil engineering; in environmental nanoscience[4] and mechanical engineering; in nanofluidics, nanofabrication, mechanical behavior of materials, nanotribology at interfaces, nanoscale energy transport[5–7]. Nanoscale engineering studies can provide advantages in areas such as energy conservation, energy storage, and lighter and more durable material. However, there are physical behaviors at nanoscales that are not fully understood, and in engineering studies where calculations at the molecular level are required, the physical behavior of the nanoscales needs to be examined and modeled.

In this thesis; the wettability of the silicon surfaces and the effect of ion concentration on heat transfer will be examined at the molecular level.

1.1. Wettability at Nanoscale

In recent years, both experimental and numerical works have been studied to research the properties of materials. In the literature, some different materials are used as surface material like etched-HMDS[8], graphene-coated silicon[9], titanium dioxide[10] and in such studies, silicon is one of the most preferred materials as surface material. Silicon has a wide range of applications like microchips, glass, biomedical. Nevertheless, due to the complex structure of the silicon and its amorphous state, it is necessary to investigate at nanoscales.

Wetting studies are prominent studies for understanding the surface tension of silicon[11]. The contact angle is a property of wettability and is found by calculating the molecular interactions of solid, liquid, and gas interfaces. The wetting angle is calculated by the dual surface tensions between these three phases. It can be written by Young's equation[12] as seen in Figure 1.1.

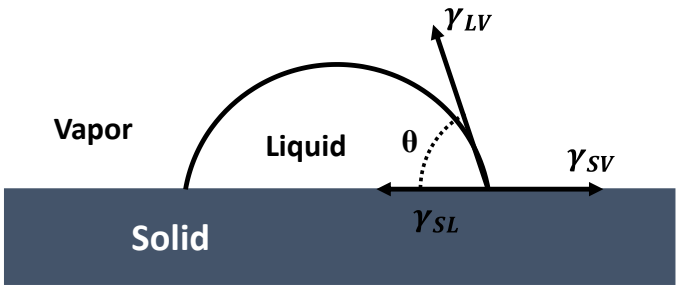

Figure 1.1. Wetting angle measurement based on surface tensions.

ɣLV, ɣSV, ɣSL, mean interfacial tension between liquid/vapor, solid/vapor, solid-liquid, respectively. θ is wetting angle and Young-Dupre equation[12] can be written depending on these parameters as (Equation 1.1):

$$\gamma_{SV} = \gamma_{SL} + \gamma_{LV} \cos\theta \tag{1.1}$$

Using this classical Young-Dupre equation gives correct results for the macro scale but, it cannot be seen precision results for the nanoscale with this equation. This is because the force interactions that can be neglected at macroscales increase the effect percentage at nanoscales. The Young-Dupre equation should be modified (Equation 1.2) because of the line tension that shows its effect more at nanoscales and that cannot be neglected[13].

$$\gamma_{SV} = \gamma_{SL} + \gamma_{LV} \cos\theta + \frac{\tau}{r_B} \tag{1.2}$$

In Equation 1.2 τ and r_B mean line tension and base radius of the droplet. According to the equation, a surface type is mainly categorized into two groups which are hydrophilic and hydrophobic surfaces. 90 degree is a critical point for this issue and it is said that contact angle is less and more than 90 degrees for hydrophilic and

hydrophobic surfaces, respectively. Additionally, super hydrophilic and superhydrophobic mean that contact angle is less than 10 degrees and more than 150 degrees, respectively. On hydrophilic surfaces, water spreads on the surface, while on hydrophobic surfaces, the water stays on the surface in the form of drops. Hydrophilic and hydrophobic surfaces are determined according to the usage area. For example; while hydrophilic surfaces provide advantages in heat transfer applications, paint and coating studies, hydrophobic surfaces are preferred in areas where water repellent properties such as corrosion are desired.

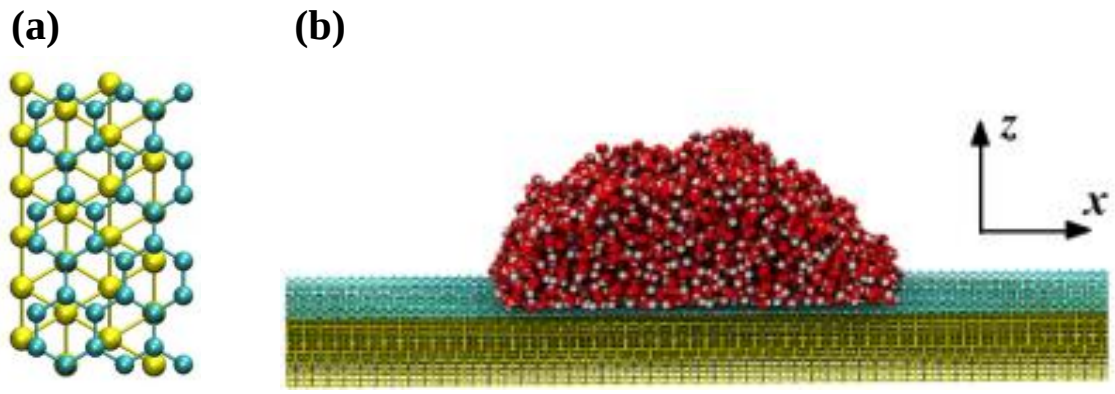

Figure 1.2. (a) Graphene coated silicon and (b) illustration of the water droplet on the graphene-coated silicon surface[9].

It is desired to be able to control the wetting behavior of the surfaces and surface coating is an application frequently used by researchers. Wetting transparency is tried to be understood by using the surface coating method. In this respect, graphene-coated materials can be given as examples as illustrated in Figure 1.2. The wetting permeability study of graphene was carried out by MD and experimentally comparatively and for the first time by Rafiee et al[14]. In their study, contact angle variation was investigated using single and multiple graphene layers on copper, gold, silicon, and glass surfaces. Although the single graphene layer acts on the glass surface, multiple graphene layers showed an effect on copper, silicon, and gold surfaces. Then, the effect of additive single and multiple CDW-grown graphene layers on the contact angle was shown by Raj et al[15]. Copper, silicon oxide, and glass were used as a surface, and while it was observed that the variation of the contact angle is greater in the single graphene layer than the coating of the surface with multiple graphene layers. Different materials were used as coatings or

layers in the literature like magnesium fluoride (MgF_2)[16], tungsten disulfide, and molybdenum disulfide[17], poly-coated surfaces[18], and molybdenum disulfide[19]. At nanoscale studies, researchers[20–22] showed that density of atoms at a solid/liquid interface cause varying wetting angle between solid and liquid. Considering wetting transparency, the effect of the solid molecule distribution near the liquid on the wetting property should be examined. In other words, solid molecules that cause wetting should be detected.

The experiments are tried to understand the connections between wetting physics and structures, but the equations developed at macro-scales do not fully solve these problems. Wetting movements take place at the nanoscale and these theories should be examined and characterized at the molecular level.

1.2. Heat Transfer at Nanoscale

Heat transfer studies are increasing day by day with the increase in production capacity and energy demand. Developments in heat transfer not only increase energy efficiency but also increase the lifetime of the materials by reducing processing times in industrial applications. Today, the cooling process is required for small-sized devices exposed to high heat such as aerospace, biomechanics, electronic components, and laser applications used in the industry. Efficient designs should be developed for heat transfer in these devices and as the size gets smaller, more careful heat calculations are required. Moreover, heat transfer at the nanoscale is a critical parameter for thermal management, efficiency, and reliability of the system. Due to their low thermal properties, high efficiency may not be obtained in new generation productions with conventional heat transfer applications. For this reason, liquid cooling is preferred in high heat applications. In the two last decades, researchers have shown that this can be avoided with nanoscale heat transfer studies. For example; critical heat flux for nanofluids, heat transfer characterization of nanofluidics, using nanofluids in a microchannel, nanofluids in space applications by Wu and Zhao[23], Mohammed et al.[24], Saidur et al.[25] and Wang and Mujumdar et al.[26], respectively.

There are two common ways to increase heat transfer efficiency; these are increasing the surface area and thermal conductivity. However, increasing the surface area due to the geometry of the materials to be designed is the second choice at the nanoscale and therefore, thermal conductivity studies are more precedent. Thermal

properties and heat transfer capabilities of nanofluids used in energy applications have gained importance. Commonly used liquid coolants like water, oil, etc. are not successful at nanoscale heat transfer applications, so adding particles are generally preferred at the nanoscale system to increase thermal conductivity. Because of the problems in the practical applications of microfluidics, these particles are generally at the nanoscale. Some parameters such as concentration, pH, and size influence the thermal conductivity of fluid at the nanoscale. To give some examples from the literature, the effect of temperature on thermal conductivity of CNT nanofluids was investigated and shown that thermal conductivity increase while temperature increased. Besides, they found a critical point for the temperature to observe linearity or nonlinearity[27]. Then, nonmetallic nanoparticles were used with a fractal model to predict effective thermal properties[28]. Not only the effective conductivity but also the effect of the volume and size of the particles on the thermal conductivity was investigated[29]. Except for conductivity studies, St-Gelais and coworkers[30] did not only analyze nanoscale heat transfer but also predicted that nanoscale heat could be converted into electrical energy. Until now academic studies about thermal conductivity is explained in this study but, understanding properties of thermal management is very important for industrial application such as computer technology, heat pipes, vehicle engines[31].

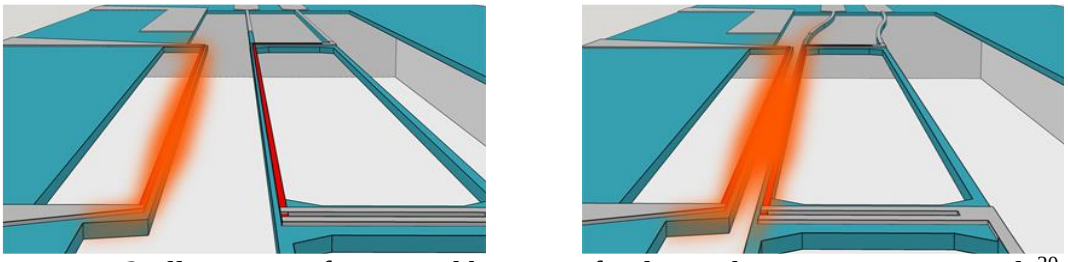

Figure 1.3. Illustration of increased heat transfer due to the gap in nanomaterials[30]

Although the thermal conductivity is increased with nanofluid in large-scale systems such as nuclear reactors, automotive, there is a thermal transport problem in nanoscale devices such as microchips. That's why, surface interactions gain great importance due to the small size of the materials at nanoscale studies. Interfacial phenomena of materials at nanoscale devices must be investigated to correct characterization of thermal resistance because, interfacial thermal resistance plays a significant role for understanding nanoscale thermal conductivity studies. In the literature,

there are some studies about between solid, liquid and gas phase interaction like that solid/liquid, liquid/gas and solid/solid interfacial thermal resistance were investigated using metallic surfaces/water, n-dodecane vapor/liquid and aluminum/silicon by Vo and Kim[32], Xie et al.[33] and Hopkins et al.[34], respectively. Researchers focus on interactions of mismatch materials in these given examples because, as presented in Figure 1.4 shows temperature jumps are observed at interface of mismatch materials by the reason of the intermolecular interactions.

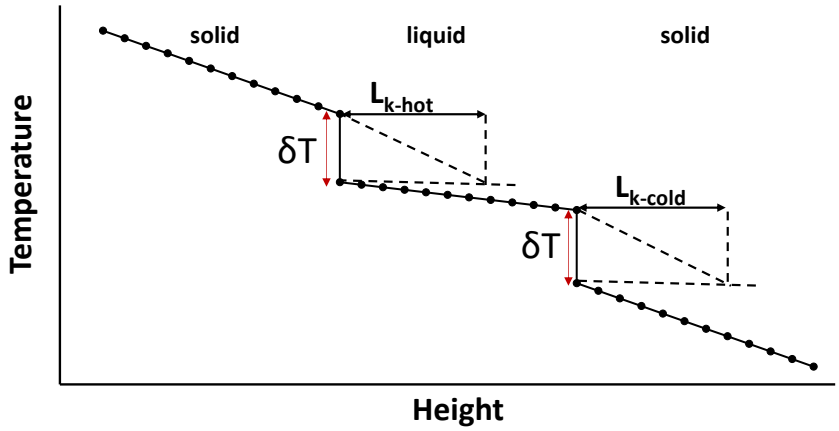

Figure 1.4. Temperature jump and Kapitza length at interfaces.

Interface thermal resistance is effective in nanoscale heat transfer studies because of the insufficient of continuum theories. It is noted that thermal boundary resistance is different from contact resistance and there is a temperature discontinuity between dissimilar materials and it is described as interface thermal resistance. Temperature jumps observed between nanoscales interfaces (see Figure 1.4) can be explained with thermal resistance. Kapitza[35] expressed the effect of the interface resistance length at solid / liquid interface in heat transfer studies, and therefore the interface thermal resistance (ITR) and thermal boundary resistance are called as Kapitza resistance. It gives some hints about near surface physical phenomena and Kapitza length (L_k) is calculated by the heat flux applied to the interface of two mismatch materials. While low ITR is desired feature for production of microelectronic devices, high ITR is desired in requirement of insulated surface as in the production of jet engines. As experimentally, Ge et al.[36] investigated thermal boundary conductance for hydrophilic and hydrophobic surfaces and they found that value of thermal boundary conductance for hydrophilic surface is higher than hydrophobic surfaces. Then, Schmidt et al.[37] showed that the interface thermal resistance

changes with surfactant concentration using CTAB coated gold nanorods. However, experimental studies have not developed enough to fully resolve at the nanoscale parameters and more theoretical study should be done at nanoscale. That's why, modelling of the system should be done at molecular level to understand interfacial phenomenon and intermolecular interactions. Numerical simulations help to calculate results before preparing experiment setup. Thermal transport between the semiconductor materials and the metal surface is especially important because it is used in the fabrication of electronic equipment and in such devices, heat must be transferred from the device. Using the molecular dynamic method, Berber et al.[38] found the thermal conductivity of the carbon nanotubes to be very high and has been the subject of research for many researchers. It has been shown that interactions in the interface of silicon, which are frequently used in microelectronics, change the thermal transport and affect the heat dissipation process. Hence, it is more accurate to perform interfacial investigation for both surface wettability and thermal transport, which affect Kapitza resistance.

Kapitza resistance or ITR calculated between the surfaces of dismatch materials can be predicted with different models, and the commonly used models are Acoustic Mismatch Model and Diffuse Mismatch Model. They predict thermal resistance at solid/liquid interface with different methods. In both models, predictions are made within the frame of phonon transfer and phonon scattering at interface is negligible in acoustic mismatch model[39], while in diffuse mismatch model[40] predict completely phonon scattering at the interfaces. Additionally, acoustic mismatch model considers high interface thermal resistance while diffuse mismatch model considers low interface thermal resistance. Information of detail of atomic level cannot predicted by using AMM and DMM. That's why, as an alternative to phonon transport, Molecular Dynamics Simulation techniques are frequently used a method at liquid / solid interface thermal resistance approach because, Molecular Dynamic Simulation works at the atomic level and it gives properties of atomic level such as chemical bond, geometry. MD continuum based also is not in need of equations and laws. In literature, most of Kapitza resistance studies at solid/liquid interface using MD can be observed. MD studies are mainly divided two groups to calculate thermal properties and these are Non-equilibrium Molecular Dynamics and Equilibrium Molecular Dynamics. Fluctuation of forces and analyze of them can be observed with using EMD. Important effects can be differentiated between large effects and minor effects with NEMD and averaging data are stored divided to bin of system. Data storage is a critical issue for MD simulations in respect to memory.

Arima et al.[41] found that results from NEMD were effective compare to EMD. They also showed thermal conductivity with fluctuations and less CPU requirements using NEMD. Additionally, NEMD is an effective algorithm for short-range interactions using in Lennard Jones. In this study, NEMD will be chosen to calculate and observe thermal properties at interface of silicon nanochannel.

As mentioned above paragraphs, silicon walls are used as solid surface for heat transfer analyzing in this study. In the literature, there are studies about water systems confined between silicon walls using molecular dynamic simulations. Yenigun and Barisik[42] were investigated effect of solid thickness on thermal properties with using silicon/water system and they found that thermal conductivity increases with increased thickness of silicon walls. In contrast, Kapitza length decreases with increasing thickness. It has been shown that the wall temperature for the silicon / water nanochannel was not cause much change in Kapitza length[43]. In the study in which the effect of thermal oscillation frequency ratio to ITR was examined, it was shown that L_K increases as thermal oscillation frequency ratio is increasing[44]. The effect of silicon added to the graphene layer on the thermal property is that when several silicones are added to the layer, the thermal conductivity increases but decreases when more than a certain number is added[45].

1.3. Electrolyte Solution

The materials that conduct electricity when it melts or dissolves in water are called electrolytes. In other saying, electrolyte solution is the solution formed by dissolving ionic compounds that dissolve into ions by dissolving in water. Conduction of the electric current occurs by the ionic compounds dissolved in water by moving the charged particles + and - in the solution. All ionic bound compounds and some polar covalent substances have electrolyte properties. For example; since there is no charge in pure water, it does not conduct. As another example is that sugar water can be given because, when the sugar water dissolves in water, it does not conduct electricity because it is separated into its molecules. Besides, acid, base and salt solution can be given as electrolyte samples. In this study, NaCl ion concentration will be used as electrolyte solution and when the salt (NaCl) solution dissolves in water, Na cation and Cl anion are formed in Equation 1.3. Electricity is conducted by the movement of Na^+ and Cl^- ions in water.

$$NaCl \rightarrow Na^{+} + Cl^{-} \quad (1.3)$$

Parameters such as zeta potential[46], electrophoretic mobility[47], EDL potential[48], electro kinetic properties[49] were investigated using different electrolyte solutions. Density of electrolyte solution.

At micro / nano scales, water/alkane interfaces were investigated under different sodium chloride concentrations using MD simulations[50]. Chowdhuri and Chandra[51] using NaCl and KCl ion concentrations that between 0 and 4.5 M investigated effect of them on electrolyte solutions by molecular dynamics. Additionally, electrolyte is so important for battery technologies. Ravikumar et al.[52] studied on effect of electrolyte concentrations on lithium ion battery with using MD simulations and they showed that diffusivity decreased as electrolyte concentration was increasing. In the study where the effect of concentration on viscosity was investigated after comparing the solution density with the experimental measurements with increasing KCl and NaCl concentration, it was shown that viscosity increased with increasing electrolyte solution concentration[53]. Then, ionic conductivity decreases while NaCl concentration is increasing[54]. Investigation of temperature effect on electrolyte solution and it's conductivity properties was presented by Taghipoor[55], investigation on effect temperature on electron transfer at solid/aqueous solution interface was done by Chidsey[56].

Until today, the effects of different electrolyte solution concentrations on diffusivity, viscosity, density, temperature, ionic conduction, thermal conduction have been frequently investigated as both experimentally and numerically. In this study, properties of electrolyte solution / solid interface will be explained by thermal properties. At molecular level, to obtain thermal properties of channel with different electrolyte solution concentration, understanding of the electrochemical properties of the solid / liquid interface is required. Unlike other studies, there are not many studies in the literature about the effect of electrolyte solution concentration on interface thermal resistance and interface thermal resistance, or called as Kapitza resistance, will be investigated under different electrolyte solution concentrations.

1.4. Surface Charge Density Effect on Heat Transfer

Surface charge at solid/liquid interface occurs by ion adsorption from the liquid phase or by ionization of chemical groups on the solid. Therefore, a potential difference arises between electrolyte solution and solid surface. Potential between solution and solid is characterized by an electrical double layer. In this study, pure silicon will be selected as a solid surface and it can easily attract with oxygen so, it acts as silica at the interface. In other saying, the hydroxyl group determines the surface charge density. Negatively charged is generally observed for silica surfaces at pH that is between 6 and 9[57]. On negatively charged solid surfaces, the positive ions in the solution are attracted to the solid surface, but short-range repulsive forces are prevented from reaching the surface. This layer, which is thought to be a molecule thickness from the surface, is known as Stern layer. In the present study, in which NaCl solution is used as electrolyte, this layer formed by ions close to the surface is called electric double layer as illustrated in Figure 1.5.

Xu et al.[58] modeled the salt electrolyte solution by placing it between two parallel silicone surfaces and applied a negative surface charge to one region of the simulation domain, which they divided into three regions, while not applying a surface charge to two regions and electric double layer is observed only in the region where there is a surface charge. EDL thickness can be explained with electrolyte concentration and Debye length is used to calculate electric double layer thickness. It has been shown by Brown et al.[59] and they presented that thickness of stern layer decreases with increased NaCl electrolyte solution concentration. EDL overlap can be prevented by the height of the silicon nano channel at the determined ion concentration and surface charge density.

Factors such as electrolyte solution, ion distribution, and pH affect the surface charge density. Although surface charge of silica has negatively charged, negatively charged on silica surface increases with increased pH[57]. Lowe and coworkers also researched importance of the first layer at interface and density was calculated with number density in the first peak. Barisik et al.[60] presented that surface charge density of silica rises when using KCl electrolyte concentration and pH increased. In another study using NaCl and KCl, it was observed that the surface charge increased as the ion concentration increased[61].

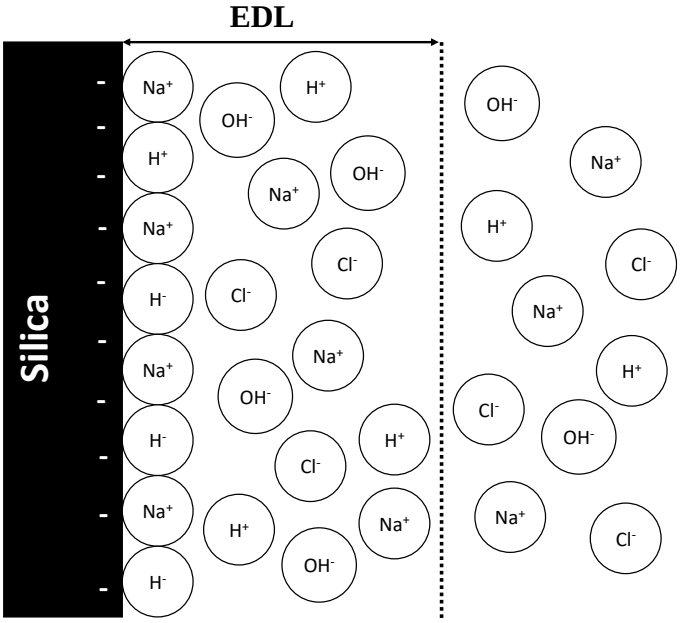

Figure 1.5. Illustration of negatively silica charged and electric double layer.

Using different potassium chloride concentrations, the effect of temperature on surface charge density has been shown and it has been observed that the surface charge density increases as temperature is increasing even though the concentrations tend to different slope with temperature[55]. The surface charge density of nanoparticles has been shown to be effective from the change in the thermal conductivity of nanofluids[62]. Furthermore, the pH value varying with the surface charge density has been shown to affect thermal conductivity[63]. In the electric field controlled heat transfer study in silicon nanochannel, it has been shown that surface charge density affects the solid / liquid interface energy. It was also observed that the heat flux increased with increasing surface charge density[64]. The maximum heat transfer rate was shown with the Nusselt number by optimizing the zeta potential with the surface charge[65].

In this thesis, different electrolyte solution concentrations will be used to investigate effect on thermal properties in silicon nanochannel and different surface charge densities of solid walls must be calculated due to concentrations. Additionally, one case will be simulated using nonionic water and then results from nonionic and different electrolyte solution concentrations cases will be correlated and thermal phenomena of nanochannel will be explained with these results.

This study is divided two parts which are wetting behavior on silicon surfaces with different planes and heat transfer of electrolyte solution filled silicon nanochannel by using Molecular Dynamic Simulations. The aim of the first part is to study an effective

molecular structure of interface region on wetting by using single crystalline silicon surfaces and amorphous silicon surfaces. For the second part, investigation on effect of ion concentration on heat transfer through silicon nanochannel is the purpose of this part. This study is divided five chapters and in Chapter 2, theoretical background and applicability of the preferred molecular dynamic simulation at nanoscale will be explained. In Chapter 3, wettability of silicon surfaces will be investigated with using crystalline and amorphous silicon surfaces. Effect of molecular distribution on contact angle will be observed and it will be explained which molecules can change wetting. In Chapter 4, Heat transfer will be investigated in the negatively charged silicon channel with electrolyte solution. The effect of NaCl concentration selected as electrolyte solution on heat transfer will be discussed. In Chapter 5, the results of all these studies will be summarized.

CHAPTER 2

MOLECULAR DYNAMICS SIMULATIONS METHOD

Molecular Dynamics studies have started to play a significant role in understanding the studies at nano scale with the increase at nano scale researches. The reasons that increase the importance of these studies are the complex and costly experimental setups of minor structures. Molecular Dynamics examines the movements of the system formed by atoms over time based on equation of motion. In other saying, MD works with Newton's second law. Each atom modeled as a point takes place in the calculations as mathematical force fields according to the quantum mechanical force and potentials, and thanks to them, the forces generated by other atoms on each atom are calculated. Net forces are used over time with Newton's equation of motion. MD studies accurately give the results of the mechanical and thermodynamic properties of the materials and thus provide information in advance for the experimental setup planned to be established[66]. Molecular Dynamic allows microscopic examinations, including atomic position and velocity, to yield macroscopic results.

2.1. Historical Background

Various methods are used in the modeling and simulation of nano particles and two of them stand out; Monte Carlo and MD Simulations. Monte Carlo is the computational technique that creates numerical solutions with the help of repetitive random samples of physical or mathematical problems whose analytical solution is impractical. This method is used various areas such as solvent molecules[67], interlayer molecular structure[68], heat transfer[69]. Molecular Dynamics Simulation, another widely used method, dates back 60 years. The Molecular Dynamics method was first applied in the late 1950s using simple computers. In the study, the phase transition for the hard sphere is modeled at the molecular level and modeling was done by taking into account the periodic condition[70]. In the 1960s, as the development of digital computers and the production of a new generation started, the studies at the molecular level started to increase. Lennard Jones potential is used to apply the Newton's second law in liquid

argon[71]. In 1967, Verlet[72] calculated the Lennard Jones potential of many particles and the equation of motion at different thermodynamics and density values. Realistically, the simulation study of liquid water by Stillinger and Rahman[73] at the molecular level is assumed to be the first Molecular Dynamic Simulation study. As mentioned in the introduction part, molecular dynamics studies are carried out in various fields from surface chemistry to aviation. Woodcock et al.[74] were simulated silica for the first time by using the BMH potential and they found some limitations of the molecular dynamic simulation method. To give an example in the field of biology, the simulation study of the protein was done by McCammon[75] in 1977. In molecular dynamics studies conducted until 1980, classical molecular dynamics method was used. In this method constant volume, constant particle number and constant energy are applied. The forces acting on atoms due to the forces arising from the interaction of atoms with each other were calculated by the potential energy functions and found by numerical analysis of equation of motion. However, since the 1980s, simulations of volume and shape change parameters have been started. The effects related to volume change were analyzed by Andersen[76] with MD and the effect of volume change was examined using constant pressure and temperature parameters. After Andersen's work, Parrinello and Rahman[77] studied the study of Andersen's work in crystal structures and interactions of pair potentials. In their study, they showed volume and shape changes with molecular simulation depending on the time. Car and Parrinello[78] have investigated a new method, the ab initio molecular simulation method, to define ionic motion. After the 1990s, researchers had studied on interaction potentials[79–81].

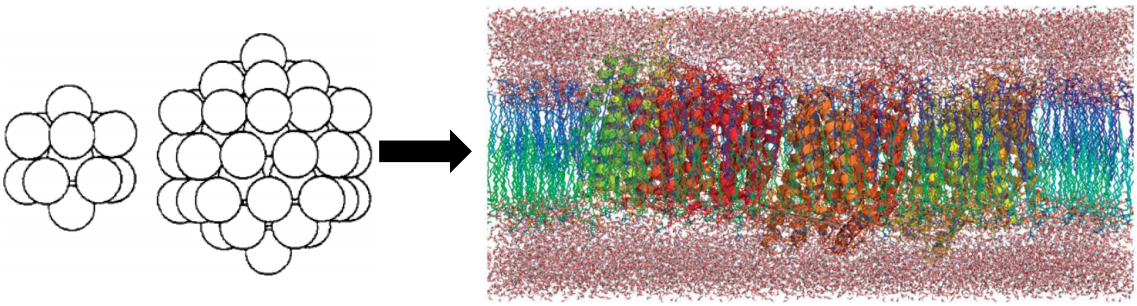

Figure 2.1. The development of modeling atoms at the molecular level[82,83].

With the developing computer technology starting from the 21st century, parallel calculation techniques have been developed in molecular dynamics studies. As shown in Figure 2.1, more atoms can be modeled in MD studies. In the 1960s, while Rahman[71] used only 864 atoms in his work, millions of atoms can be used in today's molecular dynamic simulations.

2.2. Fundamentals of Molecular Dynamics Simulations

Molecular dynamic simulations, which operate according to equation of motion and coming from quantum mechanism perform, are modelled at atomic level. As seen in Figure 2.2, experimental research gives macroscopic results while molecular dynamics studies yield microscopic results. The results obtained microscopically with molecular dynamics can be converted into macroscopic results.

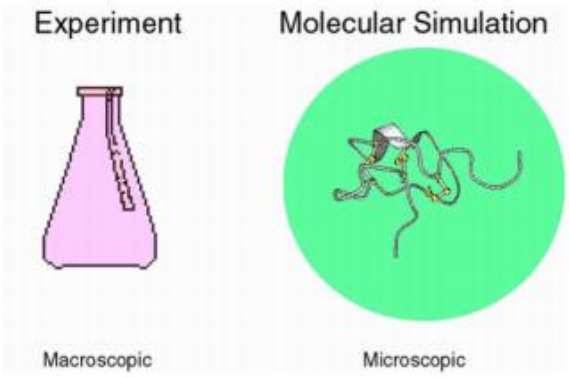

Figure 2.2. Comparison of macroscopic and microscopic results[84].

The reason for the use of molecular dynamics is the physical interactions that cannot be understood at micro / nano scales. It is very difficult to calculate mechanisms that traditional theories cannot predict using experimental methods. The reasons for this difficulty are the lack of knowledge required to design atomic level experimental systems and the expensive experiments. Molecular dynamic studies play a significant role for experimental studies in connection with the inability of the system to be ideal and easy to control and the development of new generation high quality computers. In Molecular

Dynamics studies, the desired physical behaviors are simulated after the physical model of the system is designed on the computer.

Kinds of atoms or molecules can be modelled by using MD Simulations and each atom is placed anywhere in domain. Five different types of atom in simulation box were shown in Figure 2.3.

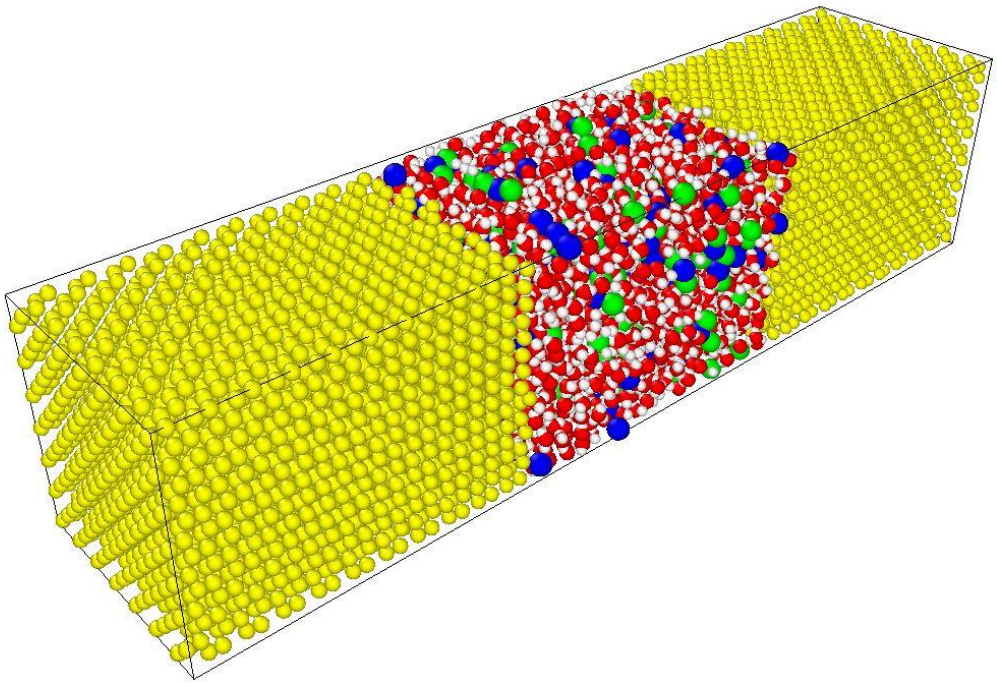

Figure 2.3. Modeling of different numbers and atoms with Molecular Dynamics.

The working principle and algorithm of Molecular Dynamics starts with modeling of the system. First, the positions and interaction parameters of the atoms are specified because MD is related to positions of the atoms, since it operates according to equation of motion. Using potential energy functions, forces between atoms are calculated and applying boundary conditions on the system. With integration of Newton's second law, velocities, forces and acceleration for the next positions of atoms are calculated. As a result of applied these steps during the steady state, statistical averages are taken for the accumulation of data. In summary, the force acting on each particle must be known to run the simulation in Equation 2.1, the gradient function should be used for potential energy in Equation 2.2 and finally acceleration is calculated in Equation 2.3.

$$F_i = m_i a_i \tag{2.1}$$

$$F_i = -\nabla_i V \tag{2.2}$$

$$-\frac{dV}{dr_i} = m_i \frac{d^2 r_i}{dt^2} \tag{2.3}$$

There is intermolecular potential due to intermolecular interaction. Intermolecular interaction can be defined with depend on distance between molecules. Atoms are affected by the average potential energy function created by all atoms in the system. Potential functions are defined summation of bonded and non-bonded potentials as seen in Equation 2.4.

$$V(R) = V_{bonded} + V_{non-bonded} \tag{2.4}$$

It can be expressed as the potential function of non-bonded atoms in two main groups, which are Van der Waals potentials and the electrostatic potentials as;

$$V_{non-bonded} = V_{Van-der-Waals} + V_{electrostatic} \tag{2.5}$$

Van der Waals forces are the bonding of atoms with weak bonds. If molecules come close to each other, repulsive forces arise and molecules cannot get closer together due to the Pauli principle. Force is required to keep the molecules together, and Lennard Jones potential is one of the most preferred Van der Waals potentials. This potential, used to denote intermolecular interaction, was first used by Lennard Jones[85]. Lennard Jones potential is characterized as function of intermolecular distance as seen in Figure 2.4.

Lennard Jones potential is related to repulsive and attraction forces, depending on whether distances between atoms are larger or smaller than radius of atoms. The Lennard Jones potential equation is given as;

$$V_{LJ} = 4\varepsilon \left[\left(\frac{\sigma}{r}\right)^{12} - \left(\frac{\sigma}{r}\right)^{6} \right] \tag{2.6}$$

In equation 2.6. ε, σ and r mean well depth, molecular diameter and distance atoms, respectively. The term Lennard Jones, whose potential is the twelfth force, refers

to the repulsive force between the two atoms, and the term that is the sixth force indicates the attractive forces between the two atoms.

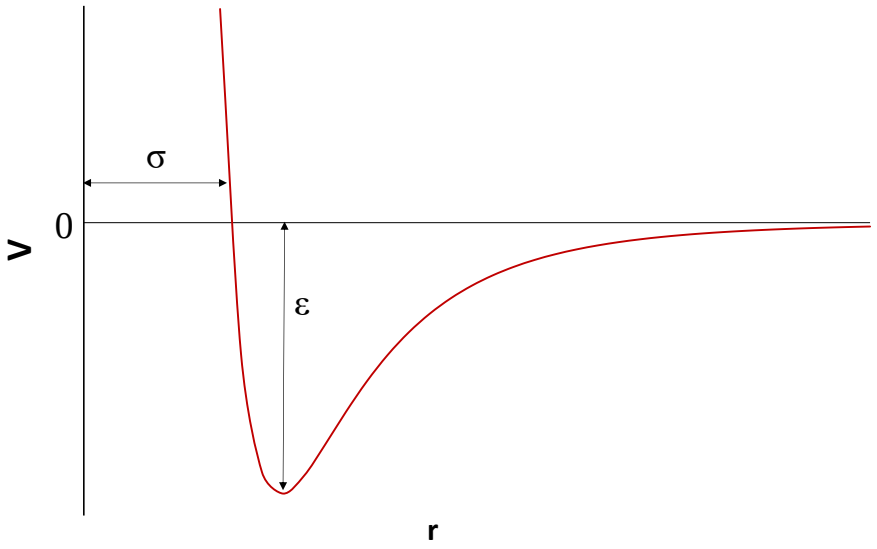

Figure 2.4. Lennard Jones potential at intermolecular distance.

The other non-bonded potential is electrostatic potential. The two charged particles apply electrical force to each other, and the interaction between these two charged particles can be found by mathematical modeling developed by Coulomb. Short range interactions are calculated with Van der Waals forces, while short and long-range electrostatic interactions are calculated with Coulomb forces. Lennard Jones and Coulomb electrostatic potential functions are used together to calculate short range interactions. Equation can also be written extended as follows.

$$V_{LJ+Electrostatic} = 4\varepsilon\left[\left(\frac{\sigma}{r}\right)^{12} - \left(\frac{\sigma}{r}\right)^{6}\right] + \frac{Cq_iq_j}{r^2} \tag{2.7}$$

The terms in the electrostatic potential that come in addition to the Lennard Jones potential; C denotes the Coulomb constant, qi and qj, the electrical charges of two different molecules in interaction state. Generally, PPPM (Particle Particle Particle Mesh) or Ewald Summation is used as two types of long range electrostatic function. Given the calculation time, the PPPM function is more useful for this study. In PPPM function, charges in the system is initially determined as 3 dimensional and system is divided small parts (mesh). Three dimensional FFT (Fast Fourier Transform) is applied then, Poisson's

equation is solved with this transform. After calculating the electric field acting on atoms with using interpolation method, electrostatic interactions that affect the atom are calculated[86].

Lennard Jones potential is mostly used for the similar type of atoms. However, there are dissimilar atom types in the system to be modeled and different methods are used to calculate the interactions between different atoms. Lorentz Berthelot mixing rule is used for dissimilar atoms[87] and for instance; silicon-oxygen interaction is calculated with using Lorentz Berthelot mixing rule and these equations is given as;

$$\sigma_{Si-O} = \frac{\sigma_{Si-Si} + \sigma_{O-O}}{2} \tag{2.8}$$

$$\varepsilon_{Si-O} = \sqrt{\varepsilon_{Si-Si} \times \varepsilon_{O-O}} \tag{2.9}$$

Lorentz Berthelot rule calculates interactions by taking simple averages. The interactions and parameters used with this rule will be shown in Chapter 3 and Chapter 4 in detail.

Different types of water models are used for molecular dynamic studies due to the physical behavior of water like specific heat, viscosity, and thermal conductivity. Any water model cannot be applied for all systems, therefore, whatever physical behaviors the water is desired in the system, the system specific water type should be modeled. Commonly used water models are Transferable Intermolecular Potential three-point (TIP3P)[88], Transferable Intermolecular Potential four-point (TIP4P)[88], Simple Point Charge (SPC)[89] and Simple Point Charge Extended (SPC/E)[89]. In addition to 4 commonly used models, Van der Spoel et al.[90] were used Simple Point Charge Reaction Field (SPC/RF) and Transferable Intermolecular Potential four-point Reaction Field (TIP4P/RF). In their study, they modeled the water with two different cutoff radii at a temperature of about 300 K and compared the properties of density, energy, dynamics and dielectric properties and consequently, they examined the system size effects on cutoff length and use of reaction field on water model. When modeling the water, after determining bond length and angle, water model type should be decided according to the number of points required. Different types of algorithm such as SETTLE[91], SHAKE[92], M-SHAKE[93], SHAPE[94], LINCS[95] algorithm is used while the water is modelling. The choice of the algorithm differs according to the system's linearity and solution form.

Due to the use of Molecular Dynamics Simulations in different and wide areas of work, various molecular dynamics software is used. Due to its complex structure different algorithms are used, and because of the points that are not fully understood in their molecular dynamic studies, software is mostly made as open source software by universities or organizations. Thanks to its open source, it is possible to access Molecular Dynamics software free of charge. Algorithms are generally developed according to science to be used. For example; Groningen Machine for Chemical Simulation (GROMACS)[96] and Chemistry at Harvard Macromolecular Mechanics (CHARMM)[97] are used for modeling biological molecules and chemistry, respectively. Apart from these, Groningen Molecular Simulation (GROMOS) developed by Groningen University, Nanoscale Molecular Dynamics (NAMD)[98] developed by University of Illinois Urbana-Champaign, Large-scale Atomic / Molecular Massively Parallel Simulator (LAMMPS)[99] developed by American National Sandia Laboratory can be given examples of software. In Turkey, Turkish Science e-Infrastructure (TRUBA) developed by TUBITAK is used by researchers[100,101]. In software like LAMMPS, the user interface is not found, as it has complex algorithms. Once the positions of molecules and interaction files are determined in the software, simulation starts.

2.3. Ensembles

Molecular Dynamics studies allow to obtain variables such as position, acceleration and speed of the system thanks to equation of motion. In molecular dynamics simulations, macroscopic variables such as pressure, volume and temperature are required in addition to the microscopic information provided. In MD studies, these macroscopic variables are called as statistical mechanics and some thermodynamics states like temperature, volume, pressure and energy are required to define ensembles.

The most used ensembles in statistical mechanics are NVE, NVT, NPT and NPH. Each letter indicates which component is fixed, for example, the components that indicate the stability in the NVE system are number of particles (N), volume (V) and energy (E). Total energy, total number of particles and total volume are conserved for NVE ensembles. For NVE ensembles, Newton's second law is applied without pressure and temperature and so, system does not allow energy transfer. In other words, energy does not change depending on time. In NVT, in contrast to NVE, energy is defined as a

function of time, and therefore energy varies with time. Because it is related to systems in thermal equilibrium, NVT is a commonly preferred type of ensemble in thermal systems.

2.4. Time Integration Algorithm

In MD studies, numerical solutions that give accuracy results are used instead of analytical solutions that do not get results due to the interconnection of the molecules' motion equations. Numerical solutions are done with the finite difference method and this method works with Newton's second law. For time integration algorithm, algorithms such as Verlet, Velocity Verlet, Predictor-Corrector, Beeman's are usually used.

All these algorithms are expressed by the derivative of the Taylor series of expansion. If t time expresses Δt time step, using Taylor expansion equations at t + Δt time position, r (t + Δt), velocity, v (t + Δt), and acceleration, a (t + Δt) vectors are calculated in Equation 2.10-11-12.

$$\vec{r}(t+\Delta t) = \vec{r} + \vec{v}(t)\Delta t + \vec{a}(t)\frac{\Delta t^2}{2} + \cdots \tag{2.10}$$

$$\vec{r}(t+\Delta t) = \vec{r} + \vec{v}(t)\Delta t + \vec{a}(t)\frac{\Delta t^2}{2} + \cdots \tag{2.11}$$

$$\vec{a}(t+\Delta t) = \vec{a} + \vec{a}'(t)\Delta t + \vec{a}''(t)\frac{\Delta t^2}{2} + \cdots \tag{2.12}$$

CHAPTER 3

WETTING BEHAVIOR OF SILICON SURFACES

Wetting is an important physical behavior that must be known in modeling liquids on solid surface in applications such as MEMS-NEMS (Micro / Nano electro mechanical system), drug delivery mechanisms, solid / liquid interface thermal resistance, sensors, and coatings[102,103]. Understanding the physical behavior of the liquid on solid surface is important for understanding the efficiency of its properties, such as the velocity and size of nanoscale systems. For these reasons, the wetting behavior of solid substrates has attracted the attention of researchers.

In recent years, wetting dynamics studies at nanoscale using Molecular Dynamics have been increasing in the literature. For nanostructures; topics such as the effect of height[104], surface roughness, and crystal structure unit dimensions[105] were investigated. In this sense, wetting and flow dynamics at micro / nano scales can be understood by calculations made with MD. Nano surface structures and water molecules can be modeled as droplets or thin films in Molecular Dynamics. In structures modeled with MD, the parameters can be controlled as desired, so that the dimensions of the surface structures and other parameters can be controlled and the wetting angle can be controlled.

In wetting studies, different materials such as graphene oxide[106], polymer surfaces[107], copper[108], titanium dioxide[109] are used as solid surfaces. Silicon[11,110] and silicon-based materials[111,112] are a semiconductor material that is widely used in characterizing studies of wetting behavior. Barisik and Beskok[11] studied on the wetting characteristic of Si (1 0 0) plane as a function of silicon-oxygen interaction strength. In their studies, the difference between vibrating and fixed surfaces has been shown and the effect of the energy parameter on the wetting angle has been investigated. In a similar study, Yen[110] observed that the contact angle decreases when interaction strength increased. Changeability of morphology of various silicon surfaces from (0 0 1) to (1 1 1) planes were investigated with respect to surface energy with using STM (Scanning Tunneling Microscopy) by Baski[113] et al. Alvarado[20] et al. calculated the contact angles on silicon surfaces in different crystal planes. They found the contact angle to be about

83 degrees for the Si (1 1 1) plane and about 103 degrees for the Si (1 0 0) plane due to the density distribution of surfaces.

In this study, the wetting dynamics of not only crystalline silicon but also of amorphous silicon will be examined. Briefly, study on the effect of molecular structure of interface region on wetting using single crystalline silicon surfaces and amorphous silicon surfaces are goal of study is to investigate Based on this, the purpose of this part of the thesis is to form unique silicon structure with homogeneous and heterogeneous densities. For this chapter, using the equations and parameters that need to be modeled on the single crystal silicon surface, the amorphous silicon surface and the water molecules placed on it, the results of the effects of contact angles, density distribution on the wetting angle will be discussed.

3.1. Molecular Dynamic Simulations Details

3.1.1. Ensembles

To study the wetting behavior, 6 different single crystal silicon structures were used and these planes were determined as Si (1 1 0), Si (1 1 1), Si (0 0 1), Si (1 1 2), Si (1 2 0), Si (0 2 1). Firstly, statistical mechanics were applied for crystalline silicon structures. Then, amorphous silicon structures were formed using crystalline silicon structure. As for the crystalline silicon plane, 6 different structures were produced for amorphous silicon structures.

First of all, simulations of single crystalline silicon structures were done with Maxwell-Boltzman velocity distribution. These simulations were started for all cases at 300 K. NVT, which means constant number of particles, volume and temperature, was applied using Nosė-Hoover thermostat at 300 K and simulation was run 2 ns to obtain thermodynamically state. Then, NVEs, which means constant number of particles, volume-energy are used as ensembles for conservation of energy of system. For all single crystalline silicon structures, periodic conditions were applied.

After the ensembles of crystalline structures, amorphous silicon structures were produced with same ensembles but different ways. Si (1 1 1) plane was chosen to produce amorphous silicon and ensemble was applied by melting then cooling. Selected silicon plane has nearly 7000 atoms. NVT and NVE ensembles were applied for melting and

cooling processes, respectively. Firstly, for the melting process, the structure was annealed to 2000 K degrees using NVT ensemble for 2 ns, then NVE ensemble was applied to the structure for 2 ns to 2000 K degrees for equilibrium. The transition of liquid to solid phase was carried out by applying a quenched operation up to 300 K degrees to the structure. In order to be consistent and improved with the experimentally measured amorphous silicon structure, the cooling rate[114] was taken as constant at 10^{12} Ks^{-1}. In this study, the height of confinement was changed while appliying melting and solidification to form different amorphous silicon structures, which have different molecular distributions. Then, a_1-Si, a_2-Si, a_3-Si, a_4-Si, a_5-Si and a_6-Si were produced as amorphous structures. Three Tersoff potential[115] was used while forming amorphous silicon structures.

The Verlet algorithm was preferred as a time integration algoritm because the advantages of Verlet are simple, efficient, stable and low CPU requirement. This algorithm was integrated into Newton's second law and was used with time step 0.001 ps. In this algorithm, new position and accelerations using current position and accelerations are calculated and they are done by backward position at time t-Δt. Velocity is calculated with using forward and backward positions.

3.1.2. Water Model on the Surface

Water molecules were placed on the silicon surface for both crystalline silicon structures and amorphous silicon structures as seen in Figure 3.1. First, the modeled 1728 water molecules were placed on the silicone surfaces. Different number of water molecule were then modeled to determine whether contact angle depends on the number of water molecule. Additionally, 1728 water molecules 5952, 4032, 3072, 2496, 960 and 576 water molecules were modeled for single crystalline silicon structures, while 3072, 2496 and 960 water molecules were modeled for amorphous silicon structures.

Some factors may be neglected depending on the size of the study. For instance, while gravity cannot be neglected at macro scales, nano-sized water droplets can be neglected when the size of droplet for water is 2-3 nm[116]. Line tension effect, which can be neglected at macroscale studies, cannot be neglected at nanoscale studies[13]. Since the contact angle at nanoscale is under the influence of line tension, water molecules were modeled taking into account the line tension. Line tension is the tension formed along the

line, not the area, at the point where three phases come together in addition to the solid, liquid and gas stresses that occur along the field in the three-dimensional system. The semi cylindrical droplet does not form curvature at three phase points, so the water droplet was placed on the silicon surface in the form of semi cylindrical to neglect line tension effect[117] as shown in Figure 3.1.

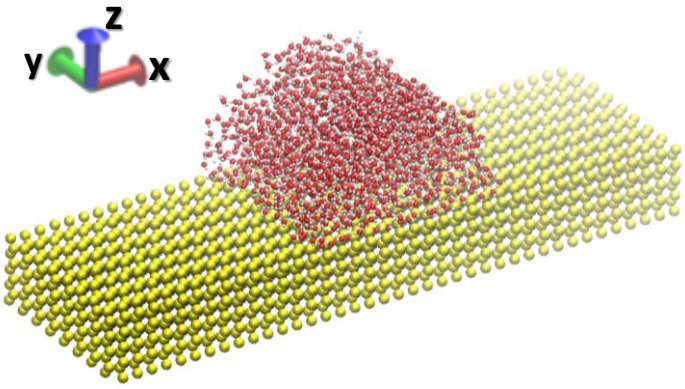

Figure 3.1. Semi cylindrical water nano droplet on the surface. Atoms present as hydrogen- white, oxygen-red and silicon-yellow.

The water model used in the simulation box is modeled according to the desired physical properties of the water in the system, and the water models are classified according to whether the water is expressed as a flexible or rigid body. During thesis, SPC/E water was selected considering the computational cost. The SHAKE algorithm was used to constrain the bond length- angle, OH bond length and H-O-H angle were taken as 0.1 nm and 109.47 °. Van der Waals at short range and Coulombic forces at long range were used to calculate the interactions between hydrogen and oxygen atoms in water. Lennard Jones potential was used to calculate Van der Waals forces. Another important point in using this water model is that the effective pair potential of Coulombic forces and L-J can be expressed with the SPC / E water model. Van der Waals and Coulombic force interactions in water molecules are defined by 1 nm cut off distance and PPPM was used as solver for long range Coulombic interactions.

The values shown in Table 3.1 were used as parameters for the Lennard Jones potential (Equation 2.7) used in the Van der Waals modeling. Table 3.1 also shows the Lorentz-Berthelot values used to find the interaction parameters of dissimilar molecules (Equation 2.8 and 2.9). Using L-B mixing rule, the interaction strength of silicon- oxygen

atoms was calculated as 0.012088 eV. However, Barisik and Beskok[11] stated that using Lorentz-Berthelot mixing rule with the parameters in the table, the interaction parameters calculated by taking simple averages cannot predict the actual interactions. 12.5% of the interaction strength value calculated using the L-B equation showed that they correspond with the contact angle values obtained by experimental results. Therefore, in this study, interaction strength of silicon- oxygen atoms was taken as ε_{Si-O}= 0.01511 eV.

Table 3.1. Molecular interaction parameters of modelling.

Molecule pair	**σ (Å)**	**ε (eV)**	**q (e)**
O-O	3.166	0.006739	-0.8476
H-H	0	0	+0.4238
Si-Si	2.095	2.168201	0
Si-O	2.633	0.01511	0

3.1.3. Modelling of Simulation Box and Calculation of Contact Angle

As a MD solver, an open source which name is LAMMPS[99] were used in this study. While modeling with LAMMPS software, general information about the scripting simulation is written. The size and boundary conditions of the simulation are specified and information about the atoms in the simulation is entered. At this stage, information such as number, type, masses, locations, lengths of bonds between atoms, angles between these atoms will be written directly to the script or written to another file and called to the script by this file. Using a silicon slab and a nanoscale water droplet simulation box was modelled. Each crystalline silicon structure has different lattice constants. Size of all simulation boxes were nearly 15 nm × 5 nm × 10 nm along x × y × z directions. Simulation boxes have periodic boundary condition in x and y directions which are the cross section areas of computational domain.

As determined in ensembles part of this chapter, six different crystalline silicon structures, which are Si (1 1 0), Si (1 1 1), Si (0 0 1), Si (1 1 2), Si (1 2 0) and Si (0 2 1) planes, were initially preferred. Like crystalline structures, six different amorphous

silicon surfaces were formed by using Si (1 1 1) single crystalline silicon plane. Then, NVT and NVE ensembles were applied to form amorphous silicon structures and these kind of amorphous structures were determined according to molecular distributions.

Contact angles are measured with using solid, liquid and gas interactions. Water density was averaged in two dimensional. The measurement technique of wetting angle is depending on base radius and droplet radius as illustrated in Figure 3.2 which also shows density contours used to measure contact angle in molecular dynamics. Thanks to the density contours, it provides an accurate contact angle measurement due to how often atoms are shown in which region. Contact angles of crystalline and amorphous silicon structures were measured with using water density contours.

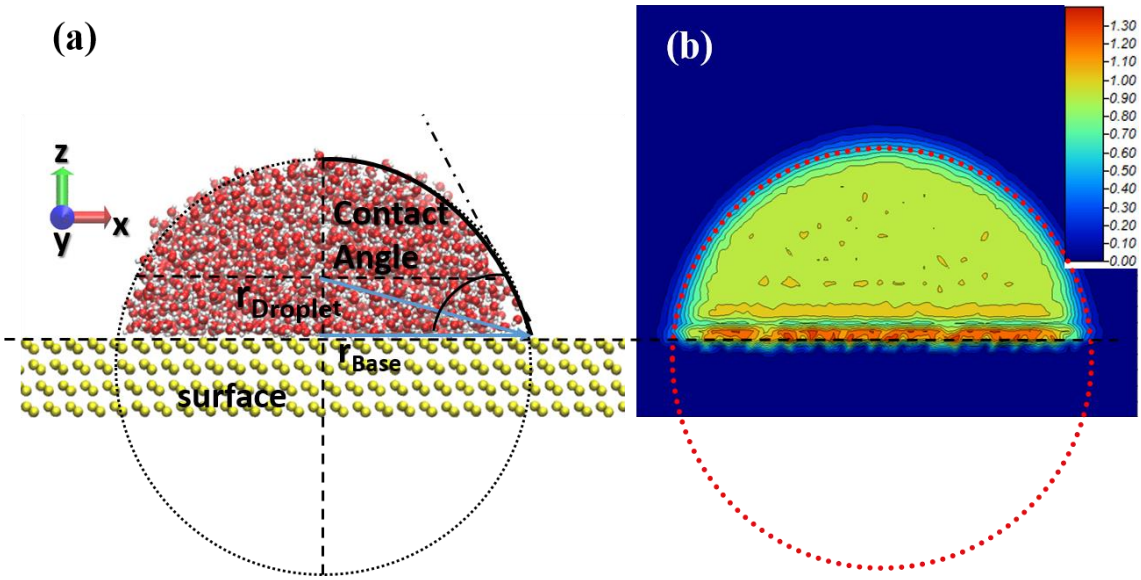

Figure 3.2. (a) Snapshot of measurement technique of contact angles, (b) water density contours.

3.2. Results and discussion

Results of contact angles of surfaces were successfully measured using cylindrical droplets to eliminate line tension effect instead of spherical droplets. Any curvature was not observed to develop for line tension effect as three phase line was linear while used semi cylindrical water nano droplets.

Contact angles of Si (1 1 0), Si (1 1 2), Si (1 1 1), Si (1 2 0), Si (0 2 1) and Si (001) crystalline planes were calculated 80.8°, 84.2°, 88.4°, 89.3°, 93.1° and 101.1°, respectively

as illustrated in Figure 3.3. Different molecular distributions were observed in solid surfaces and this solid molecular distribution has led to the measurement of different contact angles for single crystalline silicon surfaces. Interacting was maintained between water molecules and silicon atoms as constant pair-wise molecular potential but, a 20 % difference was observed in the measured contact angles of silicon surfaces due to the distributions of silicon atoms at near interface region.

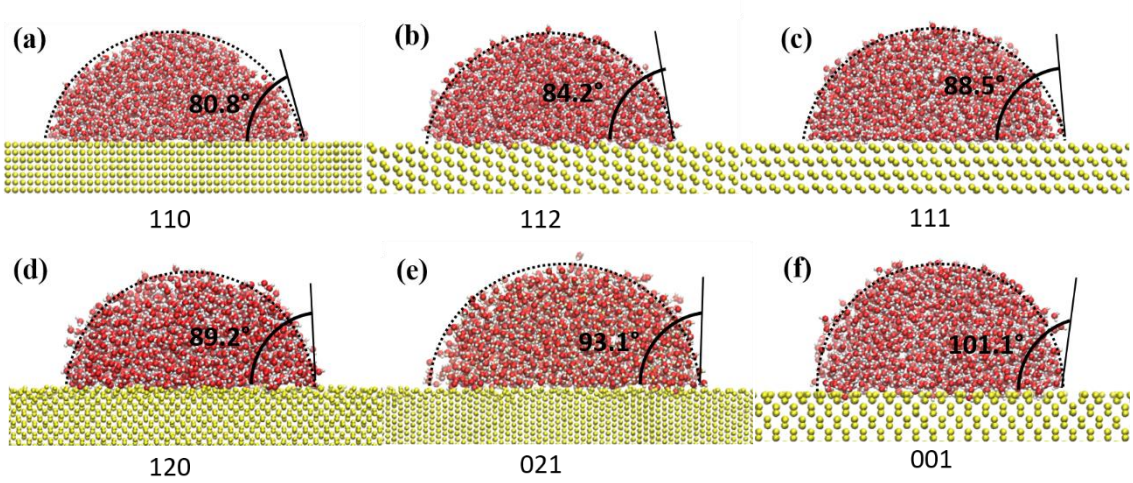

Figure 3.3. Measured of contact angles of crystalline silicon surfaces (a) Si (110), (b) Si (112), (c) Si (111), (d) Si (120), (e) Si (021) and (f) Si (001).

As determined previous parts, semi cylindrical nano water droplets were used to prevent from line tension effect. However, despite this situation, Tolman's length may cause liquid surface tension to show size-dependent development behavior. That's why, contact angles of Si (1 1 2) single crystalline silicon surface were measured while using different size cylindrical water nano droplets. The base radius of the water molecules used in different size ranges from 3.5 nm to 7.2 nm. For Si (1 1 2) crystalline plane, 5952, 4032, 3072, 2496, 960 and 576 water molecules were placed on the silicon surfaces to observe effect of Tolman's length. Contact angles were measured as 85.2°, 83.3°, 84.2°, 85.1°, 83.0°, 86.1° and 85.4° at 576, 960, 1728, 2496, 3072, 4032 and 5952 water molecules, respectively. Not much changes in measured contact angles with different size of water molecules were observed, hence, it can be said that Tolman's length was small and can be neglected in this system. Additionally, pinning effect has not been observed to vary depending on the water molecules used in different sizes.

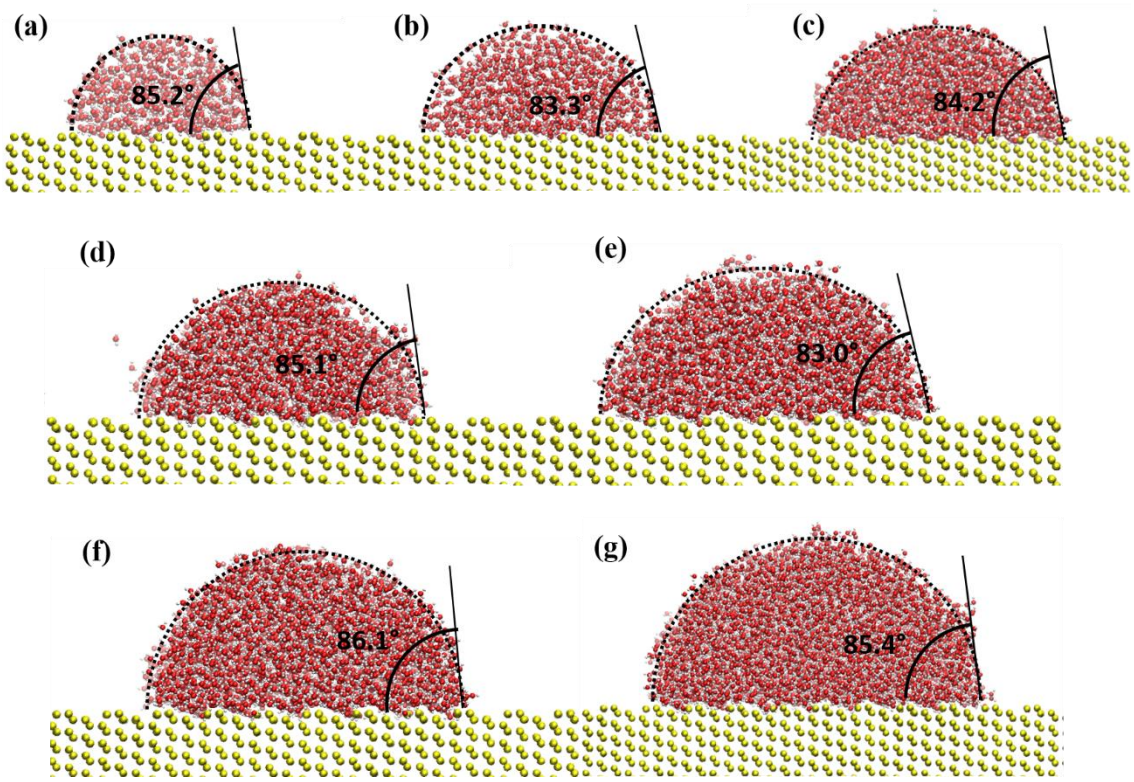

Figure 3.4. Calculated of contact angles with different size of water molecules (a) 576, (b) 960, (c) 1728, (d) 2496, (e) 3072, (f) 4032 and (g) 5952 on the Si (1 1 2) surface.

The molecular distribution causing different contact angles to be measured was investigated locally in the normal surface direction. It is done from the point of one dimensional slab bins. For all six different cases, results were plotted in surface normal directions. Zero point of height were defined at the point where solid density was zero and liquid density layering can be observed more easily in water molecules where were on the silicon surfaces[118]. The water density is expressed thermodynamically as 1000 kg/m^3, but due to the solid silicon surface, the water density cannot be observed anywhere as 1000 kg/m^3. That's why, water density at bulk was only observed in the simulation as seen in Figure 3.5. The figure also shows peaks made by crystal silicon surfaces, and high density peaks have been observed on surfaces with low contact angle measurements. The silicon density was similar to measured density experimentally[119], and as a result of the simulation, the silicon density was found to be 2330 kg/m^3. The layers of water molecules on the surface have been observed to be associated with silicon number density, and

accordingly, where the silicon density is high, it is understood that water density peaks are high.

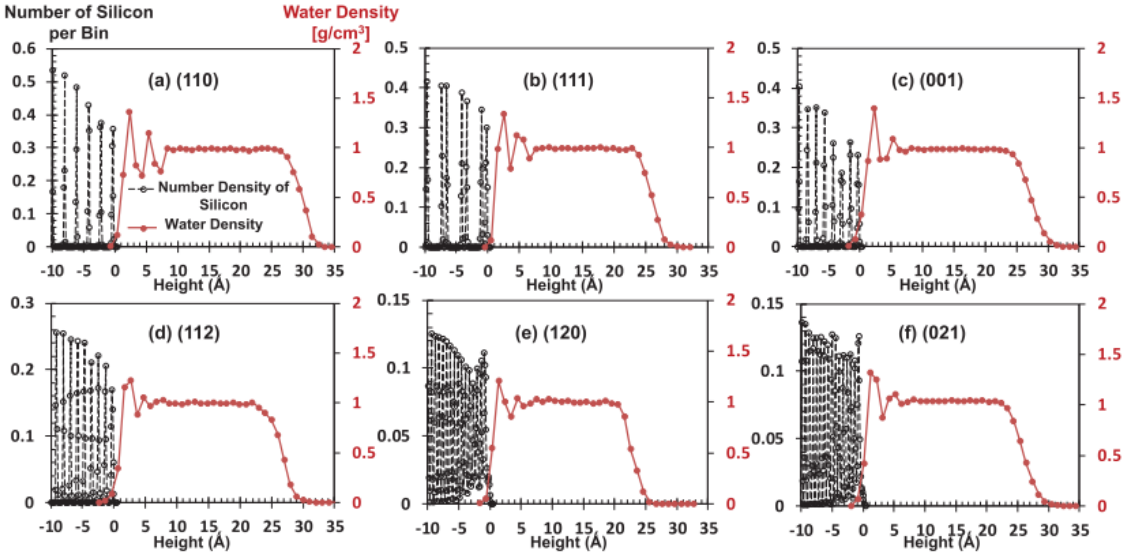

Figure 3.5. Distribution of silicon and water molecules for crystalline silicon structures. Black and red lines are number of silicon per bin and water density, respectively.

After examining the wetting behavior of crystalline silicon structures, contact angles and wetting behaviors of amorphous silicon structures were examined. Amorphous silicon surfaces were produced by applying different ensembles, first by melting and then by cooling processes. In forming amorphous structures, density is the same in each structure, while molecular distribution differs. The contact angles of the simulated silicon surfaces using 6 different amorphous silicon structures were measured and the measured contact angles were shown in Figure 3.6 as 82.0 °, 84.7 °, 86.0 °, 90.4 °, 93.1 ° and 109.5 °. The contact angles of the amorphous structures were illustrated taking into account the amorphous height, and in general, it is observed that contact angle inreases with increasing volume in the structure.

As applied on crystalline silicon surfaces, different numbers of water molecules were placed on amorphous silicon surfaces and contact angles were measured. Different number of water molecules were creating by increasing the base radius, and the relationship between the cylindrical water droplet and the contact angle was shown. Droplets with 960, 1728, 2496 and 3072 water molecules were modeled on the a_2-Si silicon surface to understand Tolman's length and pinning effect. Not much difference was observed in the measured contact angles as illustrated in Figure 3.7. Firstly, the

measured contact angle using 1728 water molecules was 84.7 °, whereas when using three other water molecules no more than 2 degrees' difference was observed. According to the measured contact angles using nano water droplet, it was understood that Tolman's length and pinning effect could be neglected for amorphous structures in this study.

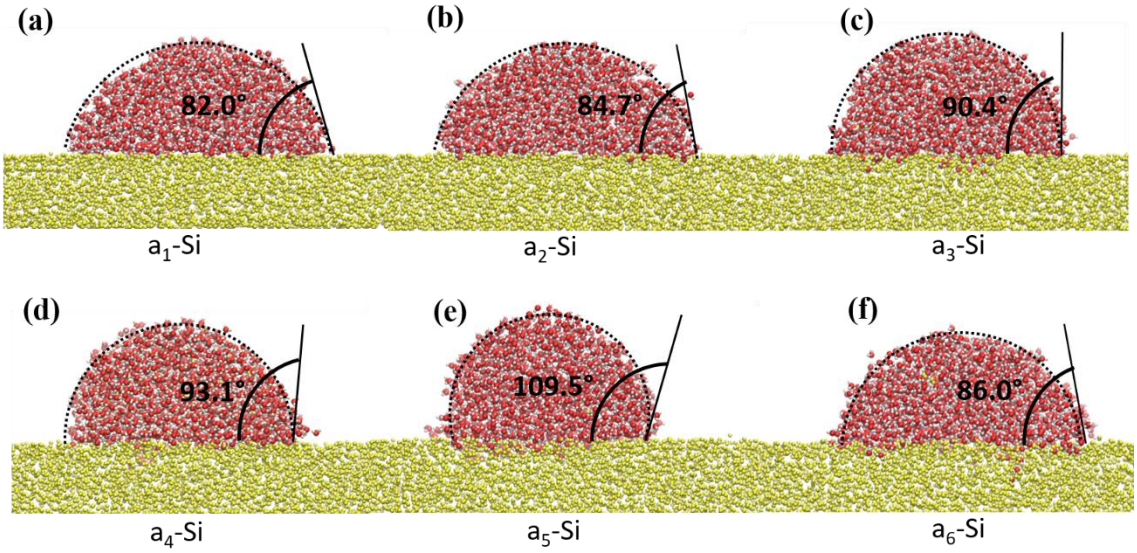

Figure 3.6. Contact angles of six different amorphous silicon structures.

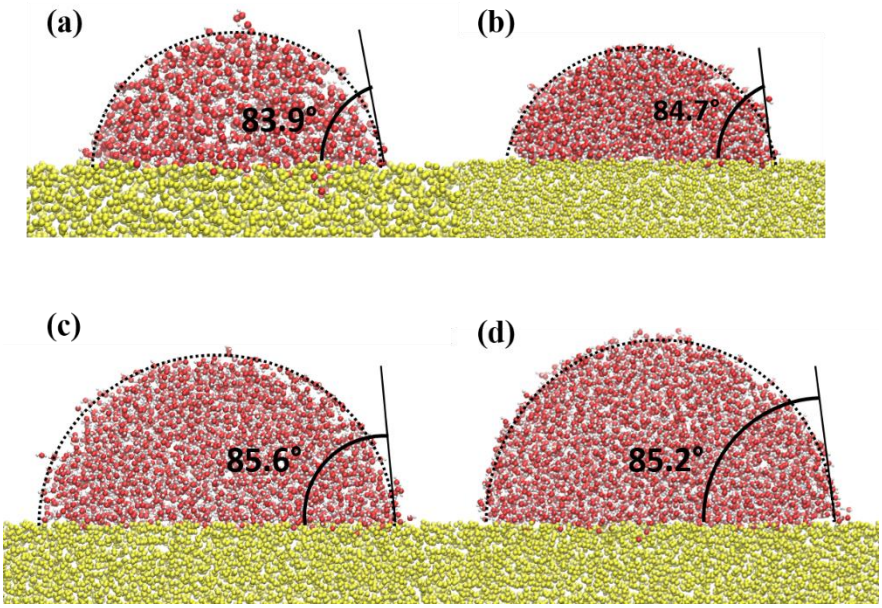

Figure 3.7. Contact angles of amorphous silicon surfaces with different size of droplet (a) 960, (b) 1728, (c) 2496 and (d) 3072 water molecules.

The contact angles enabled us to learn about the wetting properties of the structures. Observation of wetting behavior of the amorphous silicon structures can be seen with density distributions. Silicon density at the bulk has been observed as 2330 kg/m^3 and this result is acceptable[114]. Due to the random distribution of molecules in amorphous silicon structures, no high change in silicon densities was observed. As in crystalline silicon structures, for amorphous silicon structures the water density at bulk has been observed to be 1000 kg/m^3 as it moves away from the surface as shown in Figure 3.8. Increased density at interface was observed in proportion to the decrease in the height amorphisation, as in some studies in the literature[120,121]. Increasing height amorphisation allows the nano water droplet to diffuse more onto the silicon surface. Less peaks were observed in water density as seen in case of Figure 3.8 (f).

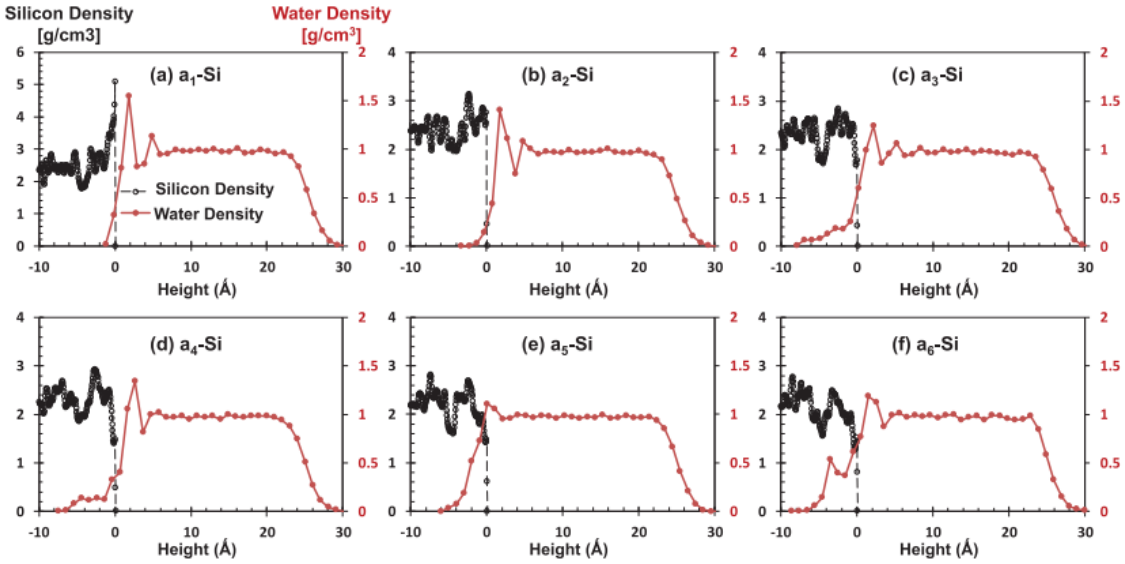

Figure 3.8. Distribution of silicon and water molecules for amorphous silicon structures. Black and red lines are silicon density and water density, respectively.

When the atomic structure and density distribution in this study were examined, it was understood to be similar to the results of experimental studies[122]. Molecular distributions of amorphous silicon structures are similar in the region called bulk at 0.5 nm from the solid silicon surface. However, molecule order differs in the near interface region. In order to better understand this behavior, parameters with different values are defined at the distance determined from the surface as 'h' as shown in Figure 3.9 (a). With 3 different h values (0.13 nm, 0.26 nm, 0.39 nm) applied, the molecular distribution and

number density were examined. Although the amorphous silicon densities were similar a bulk region for six cases, different densities were observed in the h values where were between the surface and the bulk boundary. It has been observed that where near interface density was high, it was obtained by using low h values. Also, near interface densities for the first three cases were higher than bulk density, while for other three cases, interface densities were lower than bulk density.

Figure 3.9 shows the molecular distribution and amorphous silicon structures density in the near interface region. After applying the same method for crystal silicon structures, the relationship between interface region densities and the contact angle was investigated. Figure 3.9 (a) presents 3 different h values were used as 0.13 nm, 0.39 nm, and 1 nm. Similar density values were found for crystalline and amorphous silicon structures, and accordingly, the effect on contact angles could not be observed in Figure 3.9 (b-d). However, when the h value was 0.13 nm, density calculated in the interface region varied according to the type of crystalline or amorphous silicon structure. In particular, contact angles increased when interface density decreased as presented in Figure 3.9 (b).

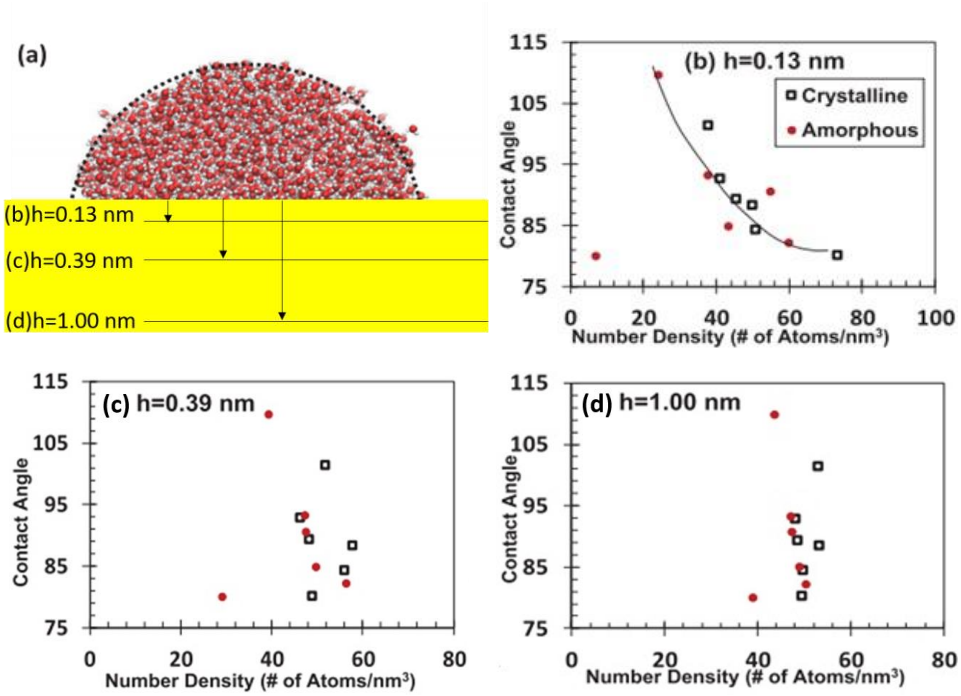

Figure 3.9. (a) Schematic representation of 3 different h values, (b-d) representation of contact angle depending on number density using different height parameters.

All in all, the purpose of this study, which is also mentioned in our article published in the journal[123], was to identify molecules that affect the contact angles of crystalline and amorphous silicon surfaces. As a result of the simulations, it was observed that the wetting behavior, such as the contact angle, is determined by molecules at a distance of 0.13 nm from the surface.

CHAPTER 4

HEAT TRANSFER OF THE ELECTROLYTE SOLUTION FILLED NANOCHANNELS

There are differences at nanoscale heat transfer studies from conventional heat transfer studies, so it attracts the attention of researchers. Nanoscale studies play a significant role in different thermal properties management for electronic, optical or new material design. For example; semiconductor silicon-silicon based materials are frequently preferred while electronic circuit components are produced[124]. In order to understand the production and physics of these materials, thermal transport properties should be investigated at nanoscale.

At nanoscale studies, the properties of materials such as thermal conductivity were investigated experimentally using methods like STM (Scanning Thermal Microscopy)[125], optical methods[126], thermal conductivity spectroscopy[127]. Modeling with the Molecular Dynamics method is frequently used in heat transfer studies at nanoscale by using computer technology, which is developed today, in order to have an important interface interactions and to observe this situation more easily. According to the purpose of use, different interface interactions gain importance at nanoscale studies such as solid/solid interfaces[128,129], liquid/gas interfaces[100], solid/liquid interfaces[131,132].

In thermal studies, it is very important to be able to define the ITR because temperature drops are observed in the heat transfer on the surfaces of dismatch materials. ITR due to the temperature jump at the interfaces is also known as Kapitza resistance[35] because, this term was discovered by him in 1940s. Kapitza defined this definition for the first time at metal liquid interface. Observed temperature jump between liquid/solid interface is written in terms of heat flux ($\vec{j}$), thermal resistance (R_K) and normal from wall ($\vec{n}$) as seen in Equation 4.1.

$$\Delta T = -R_K \vec{j}.\vec{n} \tag{4.1}$$

In this study, silicon and water were preferred as solid and liquid materials, respectively when channel was formed. However, different solid materials were used in

interface thermal resistance studies by using Molecular Dynamic Simulations such as argon-graphite and argon-silver interfaces[133], gold/water interfaces[134], argon-silicon interfaces[43]. Different heat transfer studies at nano scale can be found in the literature. For example; heat transfer was controlled by electric field and Kapitza length decreases with increased electric field[64]. Then, in the study which examined the change of interaction strength, Kapitza length decreases as interaction strength increases[135]. Kapitza length can be calculated with using different interface materials. As the density of the water increases for the silicon surface, the Kapitza length increases, but for the gold surface the length were not change considerably with water density[134].

In this study, the effect of modeled water molecules by adding ions (Na^+, Cl^-) into the silicon nanochannel will be investigated by molecular dynamic simulation method. This chapter is organized as follows; first of all, it will be explained to the studies investigating the effect of ion concentration in the literature. Then, the number of positive and negative charged ions in the ion concentration will be calculated and simulation studies of physical properties such as surface charge and density will be compared with experimental results. Finally, the effect of ion concentration on thermal properties such as temperature, Kapitza length, and thermal conductivity will be concluded. Improvements will be made according to the results found.

4.1. Effects of Ionic Concentration

In the suspension of the silicon surface with water, while the ions in the structure of the silicon come into contact with water, the silicon surface may be positive or negative ions due to the H^+ and OH^- ions contained in the water. As mentioned before, opposite charges attract each other according to Coulomb's law. Opposite charged ions accumulate around the surface in the solid diffuse region, and these layers are called as electrical double layer[136].

The electrical charge of the solid surface occurs when the solid substrate come into contact with water or solutions. At solid / liquid interface, charged ions opposite to the solid surface are observed and these opposite charges balance the electric charge. Therefore, these opposite charges on the solid / liquid interface are called counter ions. While the concentration of counter ions increases as they get closer to the surface, it

decreases as they move away from the surface and reaches the normal concentration level. In this study, different NaCl concentrations were obtained according to varying surface charge densities and quantities of sodium and chloride ions were determined according to the surface charges.

In previous works, different solutions such as KCl, NaCl, CsCl[61,137] were used as ion concentration. Qui[138] et al. modeled the water and ion concentration by placing them between the two silicon surfaces. In this study, surface charge density and ion concentration were studied in the range of -0.03 C/m^2 to -0.3 C/m^2 and 0.1 M to 4 M, respectively. It has been observed that more sodium ions approach the surface when surface charge density increased. In addition, locations where concentration peaked were observed at a distance of 0.19 nm and 0.62 nm from the surface and especially, its effect at a distance of 0.3 nm from the surface was shown. In the study in which the effect of ion concentrations on surface tensions was investigated and shown that surface tension increases as increasing ionic concentration[139].

Both experimental and simulation studies were done for investigating effect of ion concentration on thermal properties. Ozbek[140] experimentally investigated thermal properties of NaCl concentration between 20 degrees and 330 degrees. As a result of his experiment in the range of 5 M NaCl solution with pure water, it has been shown that thermal conductivity decreases with increasing NaCl concentration. It also showed that with the increase in temperature, thermal conductivity increased up to 1400 degrees and then decreased.

Rezaei et al.[141] modeled the system by using sodium chloride solution between parallel walls. The system was electrically neutralized with NaCl solution by calculating negatively charged ions on the silicon surface. They showed that the thickness of electric double layer increased as increase surface charge density and is related with ion concentration. Jelinek[142] et al. modeled the simulation box using silicon nanochannel. In the study using NaCl concentration, it has been shown that ion concentration can be controlled by temperature.

In this study, the NaCl solution in different concentrations used is the solution for each case. The average temperature in the bulk region of the silicon nanochannel is 50 degrees. Figure 4.1 shows the water NaCl phase diagram and different phases above 0 degrees are observed. To keep the NaCl concentration in solution phase, NaCl salinity in

water temperature should be around 0.1 degree and not more than 26% as seen in Figure 4.1. Therefore, in this study, the NaCl concentration was selected as the highest 4M.

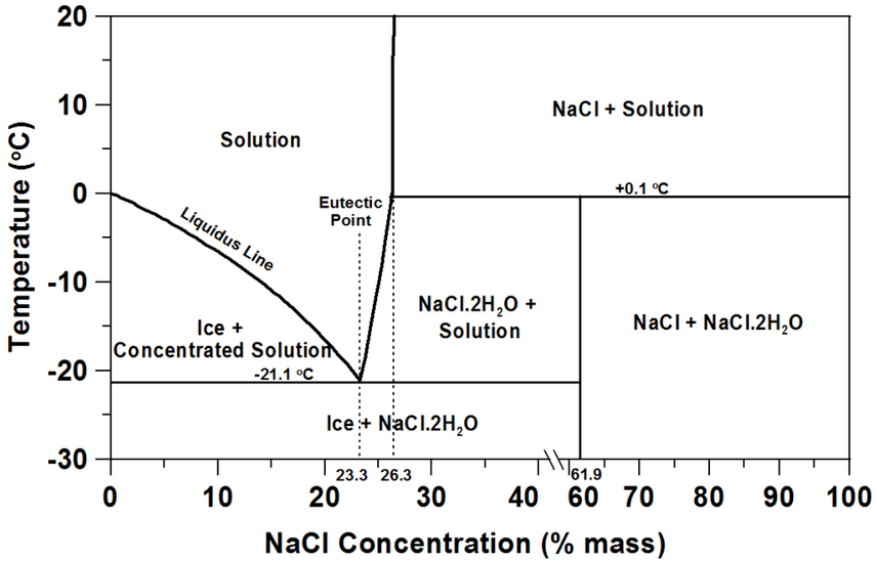

Figure 4.1. Illustration of water-NaCl solution phase diagram[143].

4.2. Molecular Dynamic Simulations Details

4.2.1. Ensembles

Silicon walls in nanochannel were formed by using Si (0 0 1) crystalline plane. Firstly, Maxwell-Boltzmann velocity distribution was used for starting simulation and NVT was applied on silicon to establish equilibrium and distribution was evolved 2 ns with Nose-Hoover and the thermostat used when creating the silicone sheets is applied to the outer layer of the simulation box for inducing heat flux. The temperature of the hot and cold silicon walls, which were called as ho-layer and co-layer, was determined 363 K and 283 K, respectively. At the same time with this stage, simulation was continued with applying NVE for all molecules.

As mentioned in Chapter 3, some properties such as simple, efficient, stable and CPU needs are easily applied to simulation domain by Verlet algorithm. The time step of Verlet algorithm integrated with Newton's second law is 0.001 ps.

4.2.2. Water Model and Simulation Domain

Simulation domain was modeled by Molecular Dynamic Simulations on three dimensional systems. Silicon nanochannel was produced by confined water and NaCl molecules between two silicon walls as shown in Figure 4.2. For such a case, simulation box was formed 16.5 nm × 3.8 nm × 3.8 nm in x × y × z directions, correspondingly. Channel height was chosen at this value to prevent electrical double layer overlap.

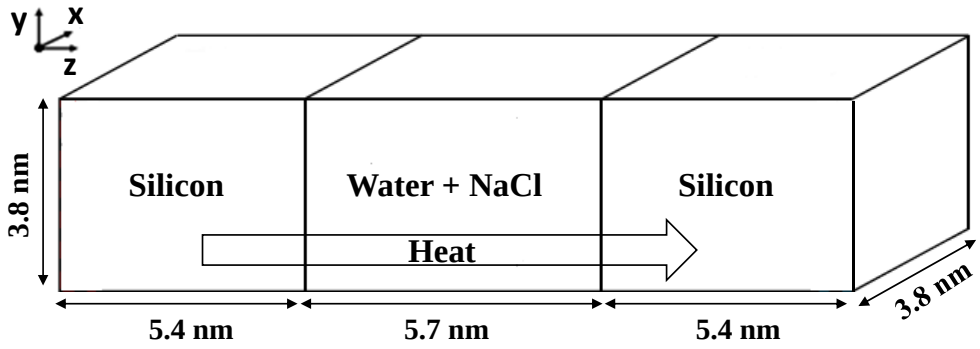

Figure 4.2. Simulation domain of silicon nanochannel.

Table 4.1. Molecular interaction parameters of silicon nanochannel.

Atom	σ (nm)	ε (kJ/mol)	q (e)
H	0	0	+0.4238
Si	0.2095	2.45	0
Cl	0.445	0.4447	-1
Na	0.257	0.06348	+1
O	0.317	0.6502	-0.8476

Various number of water molecules that were between 2473 and 2627 were used to obtain different electrolyte solution and 8036 silicon that produced by Si (0 0 1) crystalline plane was formed for all ionic concentrations. Innermost layer of silicon wall that is neighbor with electrolyte aqueous solution has 98 atoms for two sides.

SPC/E water model, which is one of the types of water models classified according to the number of the points, was chosen with the SHAKE algorithm to minimize computational cost. The SHAKE algorithm was used to constrain the bond

length and angle for OH and H-O-H, and were taken as 0.1 nm and 109.47 °, respectively. 5 atomic species which are silicone sodium, chloride, oxygen and hydrogen were used in simulations and calculation of intermolecular interactions are necessary. Hence, Lennard Jones and Coulomb potentials were used to calculate intermolecular interactions (Equation 2.7). The PPPM was used as a solver to calculate electrostatic forces in Coulomb potential. The same molecular interaction parameters with previous chapter (Table 3.1) were used for L-J potential. Unlike the previous section, sodium and chloride ions were also used when modeling the silicon nanochannel. In calculating L-J potential, Gromacs force field was used for molecular pairs of Na^{+} and Cl^{-}[144]. All molecular interaction parameters of simulation were given in Table 4.1. Then, interactions between dissimilar atoms were calculated by Lorentz-Berthelot mixing rule (Equation 2.8 and 2.9) but, the different values were used for silicon and oxygen atoms instead of the averages calculated in L-B mixing rule. In study of Barisik and Beskok[11], they showed that using L-B mixing rule, 12.5 % of the predicted result for silicon oxygen interaction was similar to experimental results.

LAMMPS was preferred as a Molecular Dynamic solver while forming NEMD (Non-equilibrium molecular dynamics) simulation. Periodic conditions were applied on simulation domain in x and y directions.

4.3. Results and Discussion

It is important to understand solid / liquid interactions in this study where the effect of ion concentration on thermal properties is investigated. In this regard, primarily the charge examination of the innermost layer of the solid wall should be carried out. Silicon was used as a solid wall for these simulations and the separation of protons in the water molecules in the channel from the hydroxyl group causes a negative charge of the innermost layer of the silicon. In other words, silicon surface has negatively charged due to fact that oxygen reacts with silicon because it acts like silica. Surface charge density can be written depending on electrolyte concentrations. Besides, number of counter ions and co-ions can be decided with surface charge and this equation given as;

$$\sigma_s = \frac{[\#_{counterions} - \#_{co-ions}]Q_C}{2A} \quad (4.1)$$

In Equation 4.1, Q_C and A mean electron charge and surface area and these were 1.6×10^{-19} and 14.44 nm^2, respectively. Figure 4.3 exhibits change in surface charge density depending on the variable pH value. Surface charge density rise when pH increased. 7 different electrolyte solutions were formed to obtain solid/liquid interactions and it was seen that not only pH affect the surface charge density, but also the electrolyte solution caused change. Figure 4.3 presents that surface charge densities increase with increased ionic concentration. These results are agreement with previous studies which are both experimentally[145] and numerically[142].

When determining the counterions and co-ions, the surface charge density at pH 7 was used for each concentration as the value of OH^- and H^+ are equal at pH 7. Thus, when the pH was 7, electrical neutrality was provided in bulk concentration. Surface charge density at pH 7 were taken as -0.0458, -0.0599, -0.0727, -0.0781, -0.0822, -0.1037 and -0.1213 C/m^2 for 0.1 M, 0.25 M, 0.5 M, 0.65 M, 1 M, 2 M and 4 M, respectively as shown in Figure 4.3. These charges cause difference between the number of counterions and co-ions and these differences increase with increased surface charge density. For example; the difference between Na^+ and Cl^- was 8 ions for 0.1 M, however this value was 22 when 4 M electrolyte concentration was prepared.

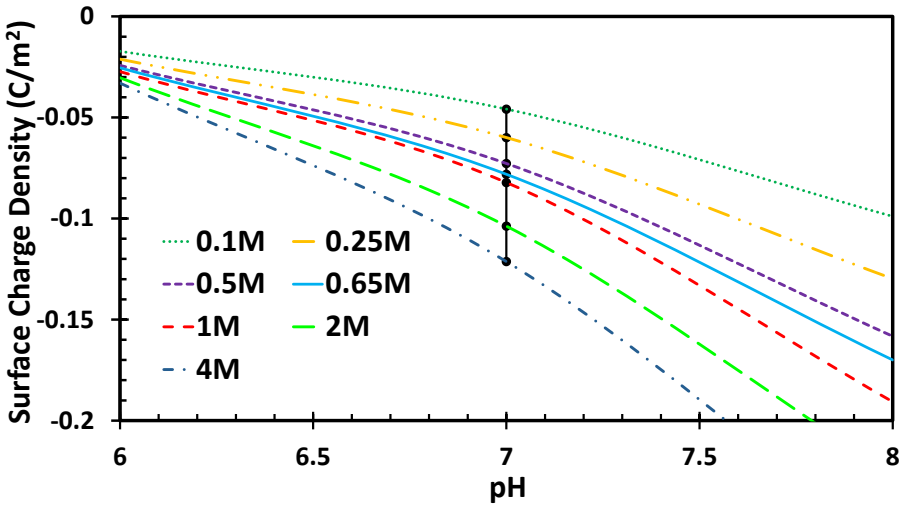

Figure 4.3. Representation of change of surface charge density depending on pH and electrolyte concentration.

The number of Na^+ ions are summation of Cl^- ions and surface charges as seen in Table 4.2. This table shows the numbers of sodium, chloride, silicon atoms and water molecules used in electrolyte concentrations when modeling simulations.

Table 4.2. The number of sodium, chloride, silicon, hydrogen-oxygen (water molecule) atoms in simulations.

Type (# of)	**nonion**	**0.1M**	**0.25M**	**0.5M**	**0.65M**	**1M**	**2M**	**4M**
Na	-	12	20	34	40	57	100	186
Cl	-	4	10	21	26	41	82	164
H_2O	2627	2485	2473	2483	2503	2514	2488	2480
Si	8036	8036	8036	8036	8036	8036	8036	8036

After determining number of sodium and chloride ions, silicon nanochannels were formed for all ionic concentrations and nonionic simulations as shown in Figure 4.4. Sodium and chloride ions in electrolyte solution were randomly placed in silicon nanochannel. Due to the surface charge density, it has been shown that more sodium and chloride ions were used in the silicon nanochannel with increasing concentration. Additionally, sodium ions at solid wall were seen and electric neutrality could be observed at bulk region in Figure 4.4.

Then, the density profiles of used different electrolyte solutions and nonionic solution were examined. Figure 4.5 presents the comparison of the density at the bulk regions modeled in simulations with experimental results. Thermodynamic states were identical for all cases and the density of water at bulk region was 988 kg/m^3. The density of solution at bulk region increase with increased salinity in electrolyte solution.

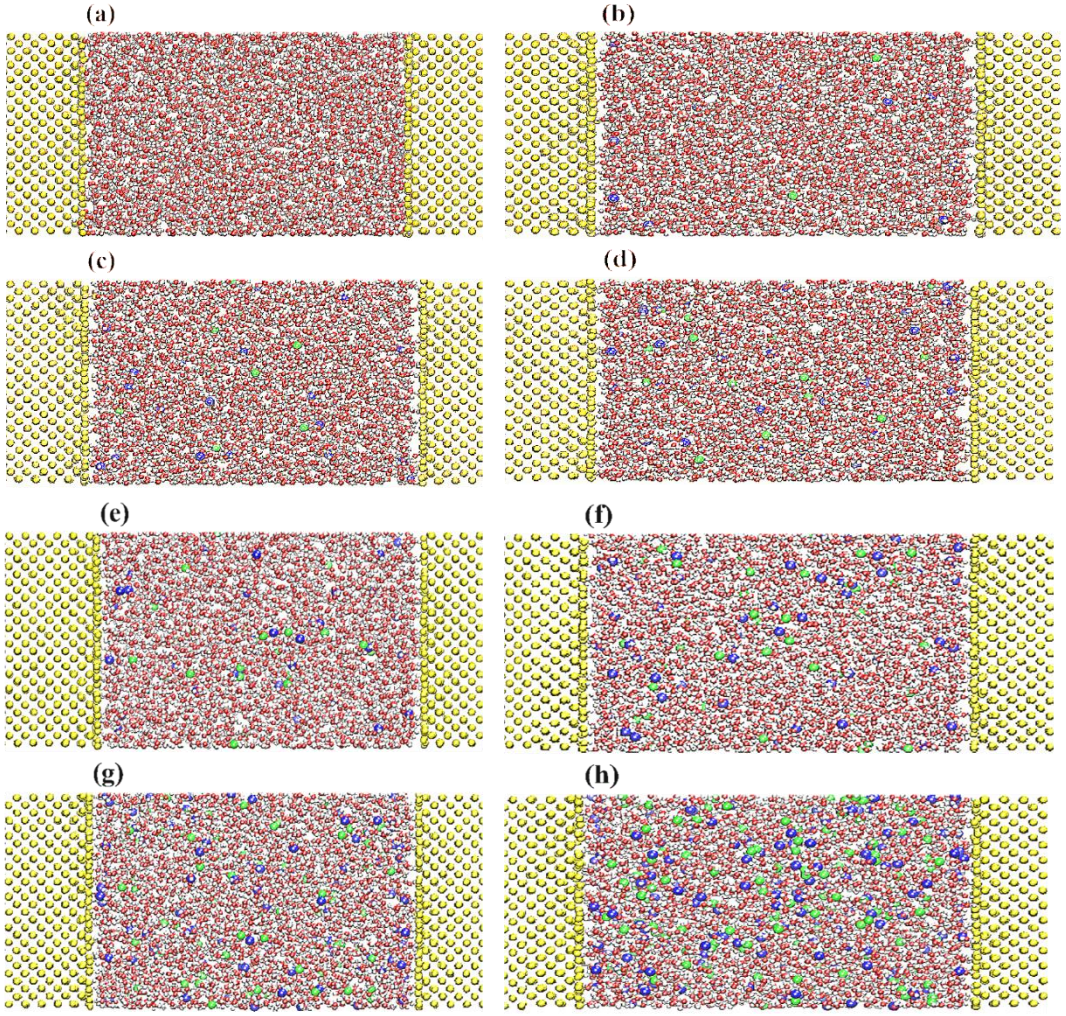

Figure 4.4. Snapshots of simulation domain for (a) nonionic case, (b) 0.1 M, (c) 0.25 M (d) 0.5 M, (e) 0.65 M, (f) 1 M, (g) 2 M and (h) 4 M. Yellow, white, red, blue and green are the color of Si, H, O, Na and Cl ions, respectively.

After illustration of density at bulk region for all cases, density profiles of water were presented under different electrolyte solutions as shown in Figure 4.6 (a). Solid/liquid interactions at wall and bulk density at the center of nanochannel could be observed with this distribution. This figure also shows water density distributions which exhibits 8 different surface charge densities. The first and second peaks of all cases were observed within nearly 5.7 nm and 6.1 nm, respectively. Because of electrostatic interactions between the surface charge at solid wall and water molecules, the movement of ions and molecules in the electrolyte solution with increasing ionic concentration has been observed. In addition, silicon density also was investigated through solid walls as illustrated in Figure 4.6 (b). The average densities were calculated as between 2.33 and 2.35 g/cm^3 and these values are in agreement as thermodynamically and literature[119].

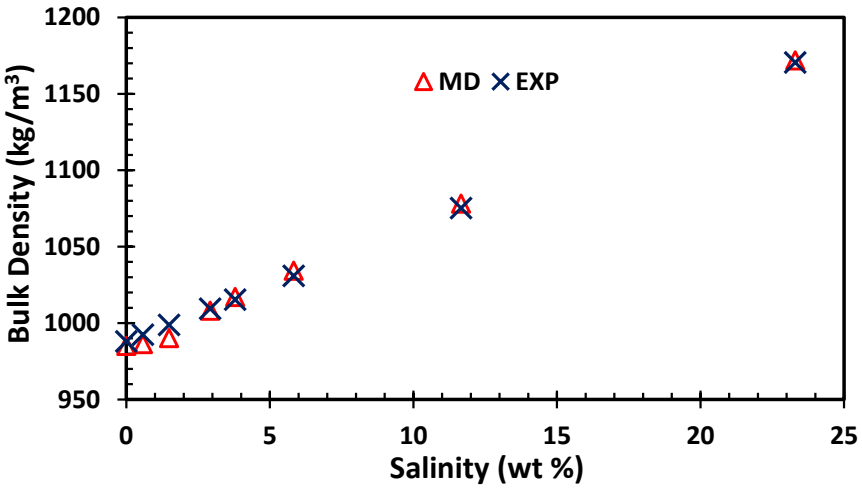

Figure 4.5. Density of electrolyte and nonionic solution at bulk region with experimentally (EXP) and molecular dynamics (MD).

Detailed electrolyte solution density profiles were shown on the hot and cold wall as illustrated in Figure 4.7 to understand effect of aqueous solution density on surfaces. The penetration of molecules in the aqueous solution into silicon surface increases with increasing ionic concentration. At the same point of the silicon nanochannel, water molecules in the 4 M electrolyte solution penetrate into the silicon more than the water molecules in the 0.1 M solution penetrate into the silicon. In this connection, Barisik and Beskok[11] have shown that the water molecules penetrate negligible into silicon at the zero electric field since the silicon surface is hydrophobic. With this figure, we showed the effect of ionic concentration on electrolyte solution density on the silicon walls with respect to density peaks. When the density profiles are examined, the peak values at the cold surfaces are higher than those at the hot surface. Besides, other parameters affect density distribution like that density peaks at first and second silicon layer increase with increased interaction strength[42].

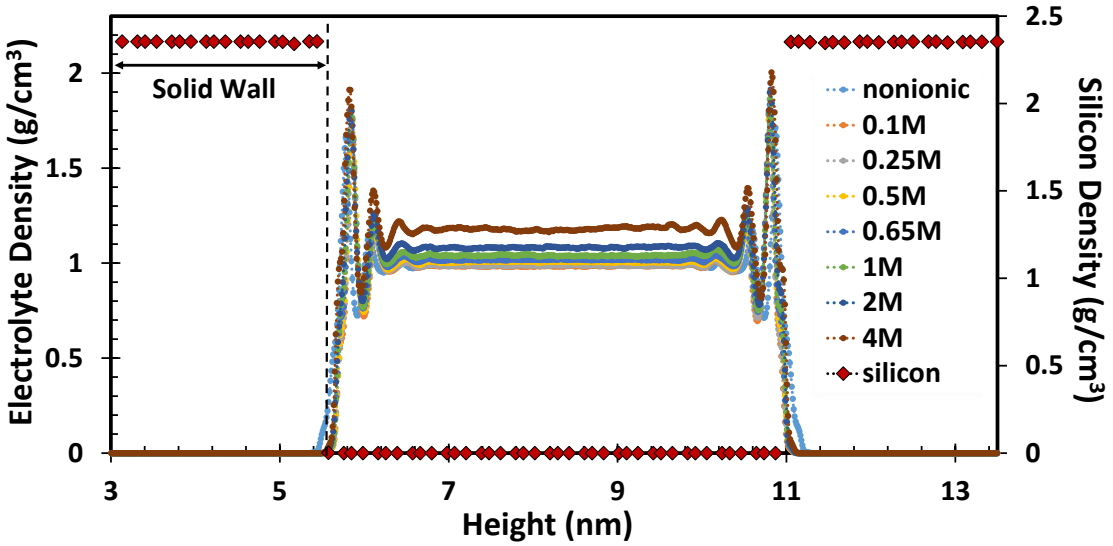

Figure 4.6. Density profiles of electrolyte aqueous solutions for different concentrations and representation of the average silicon densities at both solid and electrolyte solution.

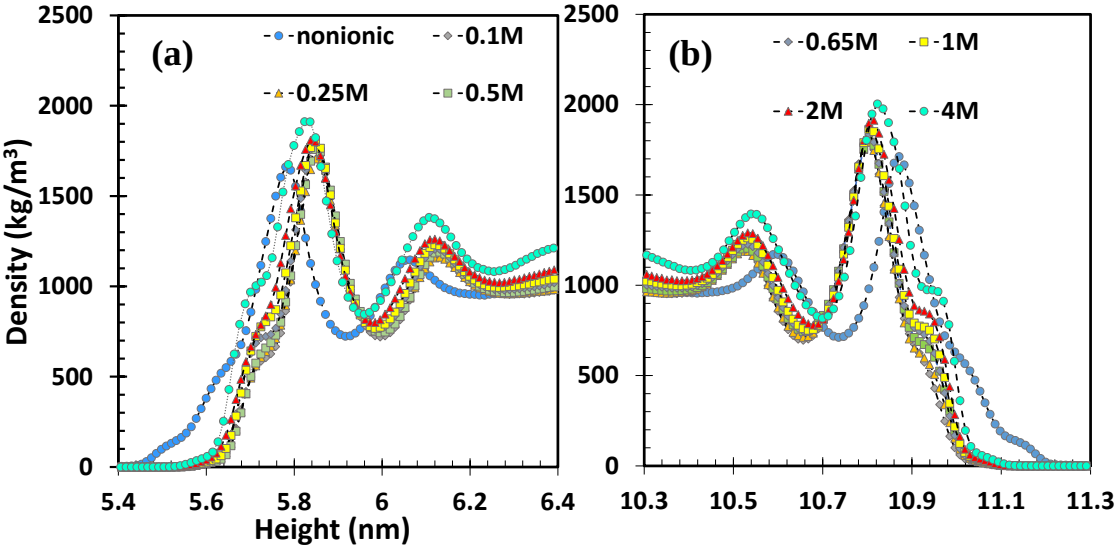

Figure 4.7. Detailed density profiles of electrolyte aqueous solutions at near (a) hot, (b) cold wall.

Next, ionic distributions of sodium and chloride ions were presented as seen in Figure 4.8. 7 different electrolyte solutions which were 0.1 M, 0.25 M, 0.5 M, 0.65 M, 1 M, 2 M and 4M were used in this study and the number of sodium and chloride ions were nearly equal to each other in the middle of the silicon nanochannel. Hence, bulk concentrations were observed for each case at this point where is at rest of the channel. In order to explain the effect of Na^+ and Cl^- in the electrolyte solution, ionic distribution

between the hot and cold wall was examined in detail as illustrated in Figure 4.9. As with the density profile, peaks close to the silicon surface were observed in the ionic distributions. However, considering the position where the sodium and chloride ions peak, these positions cannot be associated with the ion concentration and were observed at nearly 0.15 to 0.30 nm distance from solid surface. Since sodium ions penetrated closer to the silicon, the peak position of sodium ions were first observed. The reason for this is surface charge density because silicon surfaces have negatively charged.

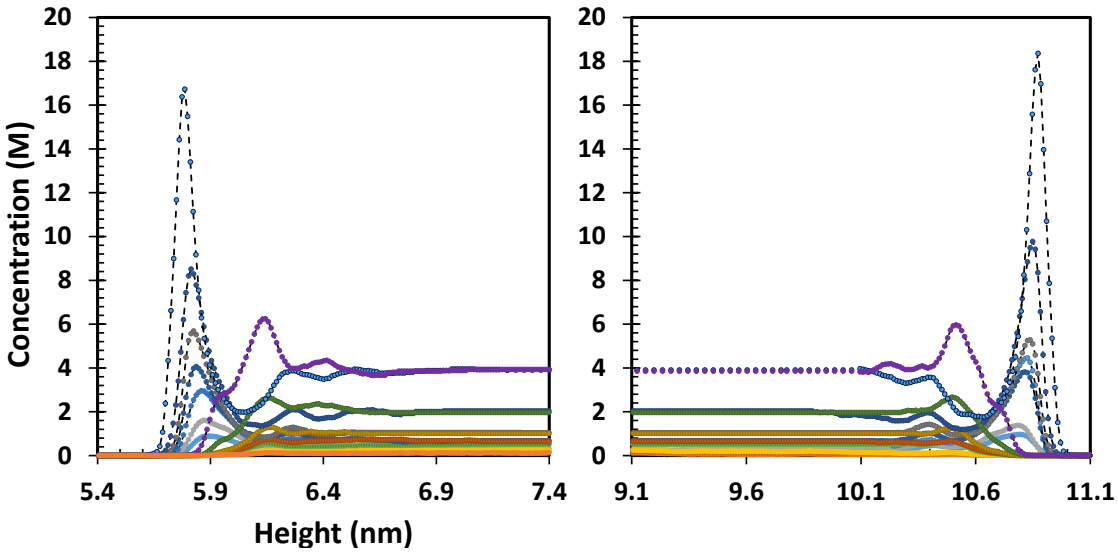

Figure 4.8. Ionic distributions of Na^+ and Cl^- under different concentrations.

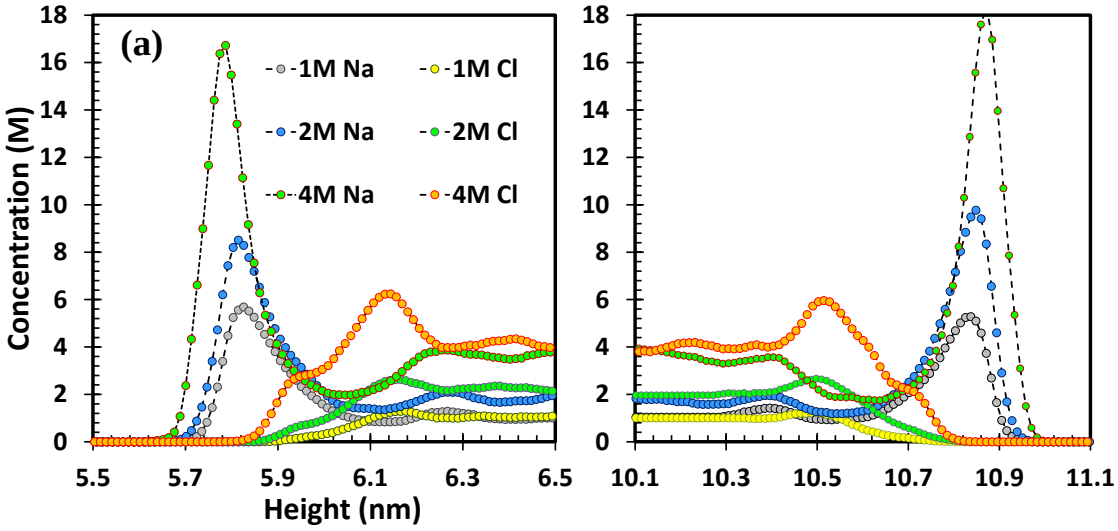

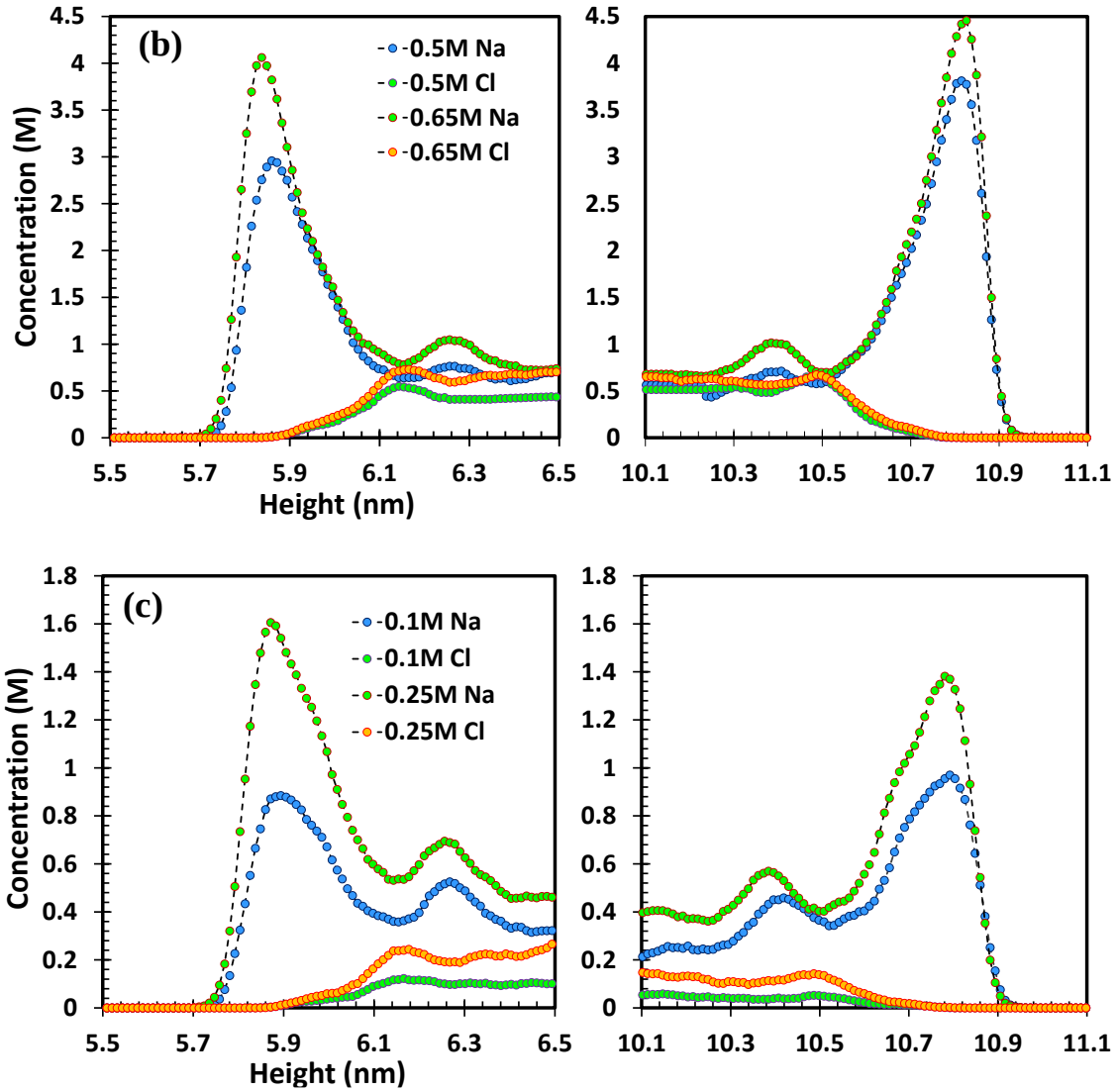

Figure 4.9. Detailed ionic distributions of (a) 4 M, 2 M and 1 M, (b) 0.65 M and 0.5 M, (c) 0.25 M and 0.1 M.

As determined above paragraph, peaks of Na^+ and Cl^- were observed for all cases but, while the peak of sodium ions in the electrolyte solution were easily observed at any concentration, the peak of chloride ions decreased with decreasing concentrations as shown in Figure 4.9 (a), (b), (c). Second peak position of Na^+ for some cases were seen and this situation can be explained with electric double layer. The first and second peaks of sodium ions were within stern and diffuse layer, respectively and peaks of chloride ions were between stern layer and diffuse layer. Recognizedly, EDL has stern and diffuse layer. As the boundary of the EDL, the position where ion concentrations of sodium and chloride can be equal accepted. At the same time, zero the electric charge density at this position can be observed[141]. With increasing concentration, counterions are much more

around the surface and the thickness of the electrical double layer decreases. These results show to us that approaches are agree with experimental study[59].

After explaining density profiles and ionic distribution through nanochannel, the effect of ionic concentration on thermal properties were studied for electrolyte solution filled in silicon nanochannel. Temperature profiles of were plotted to obtain temperature jump at solid/liquid interface and thermal properties such as thermal conductivity, Kapitza length were calculated with calculated temperature jump as seen in Figure 4.10. The hot and cold silicon surfaces were kept as 363 K and 283 K, respectively and systems were divided by 123 slab bins with size of 0.13575 nm while studying temperature distributions. Thermostat[146] was applied both hot and cold surfaces to calculate heat flux in simulation domain. Figure 4.10 shows that as expected the temperature changed linearly with the exception of solid/liquid interface region and this region gives hints for thermal properties through silicon nanochannel. Temperature jumps were observed nearly 0.16 nm and 0.11 nm away from the hot and cold surfaces, respectively. It has been observed that the temperature drop in the electrolyte solution is more linear than silicon because, the thermal conductivity of the electrolyte is less than silicon.

As explained previous paragraph, thermal properties such as Kapitza length and thermal conductivity were calculated by using temperature profiles. In the system where thermostat was applied, temperature jump and temperature gradient were used in the temperature distribution graph to calculate the thermal properties. Figure 4.11 exhibits temperature gradient at any ionic concentration. Temperature jump, ΔT, means temperature difference at solid/liquid interfaces and it has been both hot and cold walls. The temperature difference is measured by calculating the temperature gradient to the fit surface. Temperature gradient, which is symbolized as $\partial T/\partial z$, is the change of temperature depending on distance. It is used on electrolyte solutions sides and is calculated with linear equation as illustrated in Figure 4.11.

$$J = \frac{1}{V}\left(\sum_{i} e_i v_i + \sum_{i<j} f_{ij} v_{ij}\right) r_{ij} \tag{4.2}$$

$$k = q/\left(\frac{\partial T}{\partial z}\right)_{liquid} \tag{4.3}$$

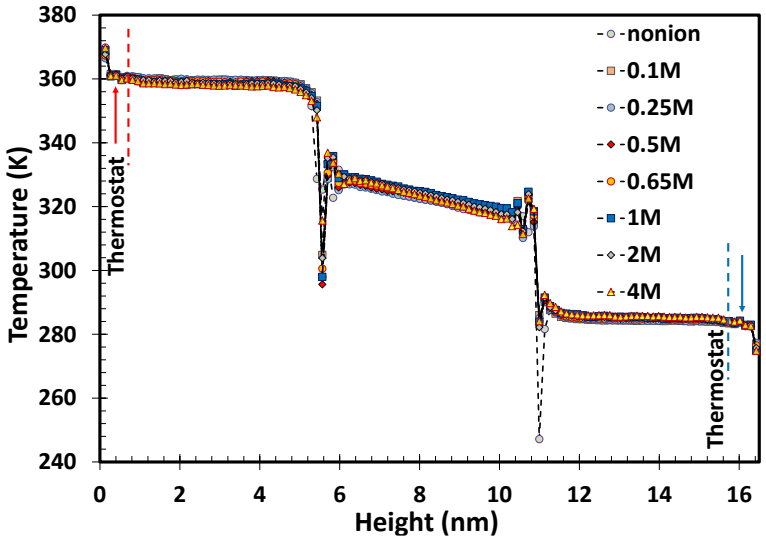

Figure 4.10. Temperature profiles of silicon nanochannel at different concentrations.

Next, thermal conductivity of all cases were calculated with using temperature gradient and heat flux (q). In order to use the heat flux correctly, it is necessary to divide the result from the molecular dynamics into the volume of the system as shown in Equation 4.2 where V, e_i, are the volume of the system, per-atom energy, respectively. Fourier's law is used for thermal conductivity of nonionic and different electrolyte solutions as seen in Equation 4.3.

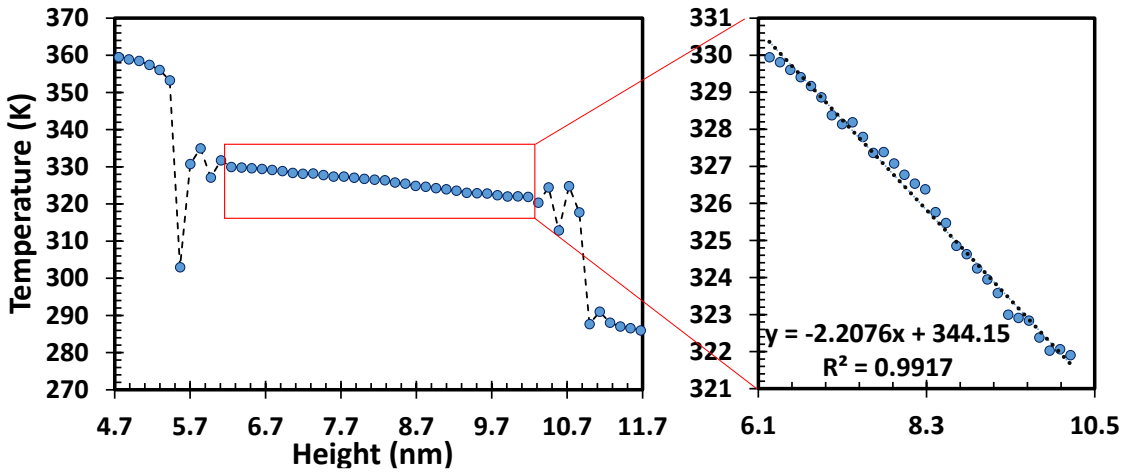

Figure 4.11. Illustration of temperature gradient at electrolyte solution.

Firstly, heat flux at different electrolyte solutions was measured to calculate thermal conductivity of electrolyte solutions then, heat flux and thermal conductivity

varying with ionic concentrations are presented in Figure 4.12. Temperature at the start of channel began with 363 K and temperature at the middle of silicon nanochannel was approximately 323 K. Heat flux increases with increased ionic concentration except at nonionic case. Explanation of nonionic case will be discussed while investigation of Kapitza length at solid/liquid interface. Figure 4.12 (b) shows that thermal conductivity of different electrolyte solutions decreases as the ionic concentration increases. The thermal conductivity of nonionic case (include of only water molecules) was found as 0.80 W/mK and this result was in agreement with previous works in the literature[64,147].

In terms of thermal conductivity, nearly 20% difference was observed between the highest concentration of 4 M and nonionic case. While a linear decrease was observed up to 1 M, less decrease in thermal conductivity was observed from 2 M. Adding sodium and chloride ions into the electrolyte solution causes reduced thermal conductivity due to weak intermolecular interactions between ions in NaCl and water molecules. Besides this is because, ionic mobility decreases with increased concentration. With respect to thermal conductivity of silicon, thermal conductivity of electrolyte solution is less than silicon and it affects temperature gradient, hence more linear temperature gradient were observed for electrolyte than silicon as seen in Figure 4.10.

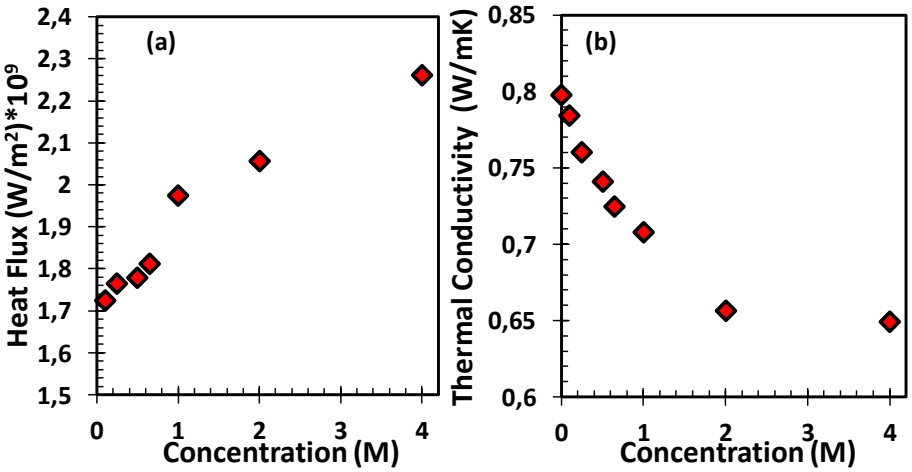

Figure 4.12. Varying with ionic concentration (a) heat flux and (b) thermal conductivity of electrolyte solutions.

Temperature jumps are observed at the interfaces of dissimilar materials and Kapitza length is used to characterize the interface thermal resistance. In this study,

Kapitza length was observed at silicon/electrolyte interface and was calculated as seen in Equation 4.4.

$$L_k = \Delta T / (\frac{\partial T}{\partial z})_{liquid} \quad (4.4)$$

where ΔT is the temperature difference between solid and electrolyte solution, $\Delta T = T_{electrolyte} - T_{wall}$, $\partial T/\partial z$ is the temperature gradient at electrolyte solution. Thermal resistance length or called as Kapitza length (L_K) were shown in varying ionic concentrations for both hot wall and cold wall as seen in Figure 4.13. In all concentrations, L_K at cold surface is higher than L_K at hot surface, and both L_K cold and L_K hot decrease with increased ionic concentration. In literature, Barisik and Beskok[135] investigated effect of interaction parameters on interface thermal resistance and they found that L_K at cold surface is higher than L_K hot surface for $\varepsilon_{Si-O}/\varepsilon^*_{Si-O} < 0.2$. The temperature difference is determined by thermostat is similar for all cases and the temperature gradient in the electrolyte solution has affected the results. The reason is that temperature drop in electrolyte solution was easily observed as linearly with increased ion concentration. Furthermore, temperature gradient increase as interface thermal resistance decreases.

Contact angle increases with decreased interaction strength, hence solid surface acts as hydrophobic[11] and according to the interaction strength value used in this study, the solid/liquid interface behaves as hydrophobic. Measured Kapitza lengths at hydrophobic solid/liquid interface were between 7.50 nm and 13.50 nm and agreement in other molecular dynamics[135,148] and experimental studies[149].

Considering the electrolyte solution, a trend of Kapitza length at varying concentrations could be observed and thermal resistance length decreases with increased ionic concentration. Nonionic case should be examined since it is not compatible with trend. For the nonionic case due to its long range interaction, it cannot be said that it is included in the trend. In other words, this situation was observed due to the long range interaction of ions added into the water molecules. It will also be seen at an electrolyte concentration of less than 0.1 M, both Kapitza length for hot and cold wall and the heat flux will differ from the nonionic case. The results will agree with the ion concentration trend. Density profiles presented in Figure 4.7 was examined to understand an outlier and showed that for the nonionic case, the water molecules peaked and penetrated into the

silicon, whereas the position was closer than other cases. In addition, the temperature gradient value was similar to that of 1 M electrolyte. That's why, density influenced on heat flux and Kapitza length of nonionic case.

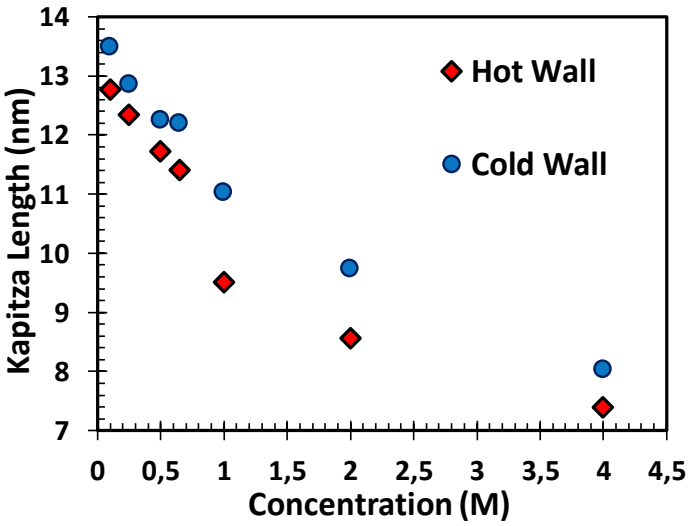

Figure 4.13. Kapitza lengths depending on the variation of electrolyte concentration.

As a result, density distribution, surface charge density, temperature profiles, temperature jump, temperature gradient, heat flux, thermal conductivity and Kapitza length were determined with ionic concentrations. Thermal conductivity and Kapitza length decrease while the temperature gradient, surface charge density, heat flux, density of electrolyte solution increase with increased ionic concentration.

CHAPTER 5

SUMMARY AND CONCLUSION

With the development of computer, material and manufacturing technologies, studies in small sized has increased by the researchers in the last two decades. It has been observed that traditional theories cannot always explain the physics in materials like wetting and thermal management as the size come to nanoscale. Accordingly, surface interactions at atomic-molecular level play an important role in these nanoscale studies and interface interactions between mediums should be investigated. Therefore, in this study, wetting and heat transfer behaviors were studied at nanoscale by considering solid / liquid interface phenomena. This thesis, where silicon is frequently used as a surface material in microelectronic applications, is divided into two as the main titles; firstly, the wetting physics of the nano water droplets on the silicon surface and the investigation of effect of the electrolyte solution in the silicon nanochannel on the heat transfer.

In Chapter 2, information about Molecular Dynamics was given in detail because, MD Simulations based on equation of motion were used for modeling at the molecular level with LAMMPS solver in this study. SPC/E water models with SHAKE algorithm were preferred when water molecules that on the surface and in the nanochannel was modelled. While Lennard Jones and Coulombic potentials was used to calculate the molecular interactions between hydrogen-oxygen atoms in water molecules and ions in electrolyte solution. The Lorentz-Berthelot mixing rule was used to interact with different atoms such as the interaction of silicon and hydrogen atoms. Instead of mixing rule for silicon and oxygen atom interaction, the value whose accuracy was specified in the literature[11] was preferred. As long range forces PPPM (Particle Particle Particle Mesh) solver was used in simulations.

In Chapter 3, as a first step water droplets on silicon surface were modelled to understand wetting behavior. The aim of chapter is to characterize effective range of intermolecular forces for wetting. For this reason, six different type of single crystalline and six amorphous silicon structures formed from crystalline silicon with various number of the water molecules were used during simulations. Similar surface density ranges that

high and low were chosen for both crystalline and amorphous silicon structures. One of the critical point of this study is that nano water droplets were formed as semi cylindrical to eliminate line tension effects while modelling of the system. The measured contact angles range from 80.8° to 109.5°. This difference is due to solid molecules distribution of the surface. Although semi-cylindrical water droplet is used, Tolman length effect can be seen. However, in order to see the effect of Tolman length in this study, different water molecules were modeled on the silicon surfaces in varying base radii of the water droplet. The contact angles of the crystal and amorphous surfaces of different water molecules used were similar and it was shown that Tolman length could be neglected. In order to characterize the factors causing the change of contact angles, near interface region has been defined at determined distances away from the surface. First, near interface height parameters that are smaller than the bulk area in amorphous silicon structures were specified and in regions at 0.13, 0.26 and 0.39 nm away from the surface, number density was compared with bulk region density. Bulk region density was similar for different amorphous structures. However, as h increases, number density increases for some amorphous silicon structures and decreases in others. Then, near interface density was calculated for single crystalline silicon structures and contact angles were measured various h parameters as a function of number density. In the study examined using 3 different h parameters, number density was similar at the interfaces that extending 0.39 and 1 nm from the surface and it was observed that it did not much affect the change of contact angle. In contrast, the interface at one or two atomic diameter distances from the surface has been shown to determine wetting physics. The change of the contact angle and wetting behavior can be explained especially by the silicon solid structure at the interface 0.13 nm from the surface both single crystalline and amorphous silicon structures.

In Chapter 4, after investigation of wetting behavior at near interface region, the nanochannel was modeled as confined electrolyte solution between two parallel silicon walls. The effect of various electrolyte concentrations on thermal properties which are heat flux, temperature gradient, thermal conductivity, interface thermal resistance and temperature jump were investigated by using physical chemistry properties at solid/liquid interfaces such as density distribution, ion distribution. By determining surface charge density of negatively charged silicon at different concentrations used, the number of Na^+ and Cl^- ions used for concentrations were calculated. After the simulations, the vicinity

of the ions in the electrolyte solution with the solid wall were shown. Thereafter densities of the silicon / solution / silicon system at bulk region were compared by the density values found by experimental results, the distribution in the density profile at solid / liquid interface was examined. It was observed that the atoms and molecules in the electrolyte solution penetrated into the silicon atom without any gap with solid wall. Penetration of water molecules into silicon atoms are related that shown structure of solid and wall-fluid interaction by Vo and Kim[148]. Five different metallic materials that are FCC lattice and diamond lattice structure were used in their study and they concluded that water molecules penetrate into silicon atoms in first layer without gap with solid wall. This is because, APF of silicon diamond lattice structure is 0.34 and is smaller than Atomic Packing Factor of 0.74 for FCC lattice. Moreover, first peaks of silicon are lower than FCC structures. Based on this study, strong or weak solid / liquid interaction from liquid / liquid interaction affects density distribution. As a result, as ionic concentration increases, the first peak of electrolyte solution is closer to the silicon wall. Then, ion distribution was examined to obtain information about the thickness of the electric double layer. Since silicon interacts with oxygen atoms in water molecules, a negative surface charge occurs at solid / liquid interface then, EDL is observed on the surfaces. EDL thickness decreases with increased electrolyte solution concentration. Next, temperature distribution was plotted to calculate thermal properties at solid/liquid interface and electrolyte using some terms such as temperature gradient, temperature jump and these terms were shown as detailed in temperature profile. Similar temperature differences were observed between the wall and the electrolyte whereas the temperature gradient in electrolyte rises with increased ion concentration. Least square fit was applied on liquid (electrolyte solution) to calculate the observed temperature difference due to the interaction between dissimilar atoms. As shown in Equation 4.4, thermal conductivity and temperature gradient are inversely proportional. Therefore, conductivity drops while temperature gradient increases as electrolyte concentration was increasing. Kapitza lengths were calculated to characterize the interface thermal resistance both hot and cold walls. Calculated results were agree with molecular dynamic simulation and experimental studies. In consequence, L_K for hot surface is smaller than L_K for cold surface and Kapitza length at solid/liquid interface decreases with increased ionic concentration enhancing the heat flux and heat transfer.

REFERENCES

(1) Baranova, E. A.; Bock, C.; Ilin, D.; Wang, D.; MacDougall, B. (2006) Infrared Spectroscopy on Size-Controlled Synthesized Pt-Based Nano-Catalysts. *Surf. Sci. 600* (17), 3502–3511. https://doi.org/10.1016/j.susc.2006.07.005.

(2) Christopher, P.; Linic, S. (2008) Engineering Selectivity in Heterogeneous Catalysis: The Impact of Ag Surface Structure on Ethylene Epoxidation Selectivity. *AIChE Annu. Meet. Conf. Proc.* No. 100, 11264–11265.

(3) Xia, F.; Wang, H.; Xiao, D.; Dubey, M.; Ramasubramaniam, A. (2014) Two-Dimensional Material Nanophotonics. *Nat. Photonics*. https://doi.org/10.1038/nphoton.2014.271.

(4) Kamat, P. V.; Meisel, D. (2003) Nanoscience Opportunities in Environmental Remediation. *Comptes Rendus Chim. 6* (8–10), 999–1007. https://doi.org/10.1016/j.crci.2003.06.005.

(5) Farsad, M.; Vernerey, F. J.; Park, H. S. (2010) An Extended Finite Element/Level Set Method to Study Surface Effects on the Mechanical Behavior and Properties of Nanomaterials. *Int. J. Numer. Methods Eng.* https://doi.org/10.1002/nme.2946.

(6) Bhushan, B.; Jung, Y. C. (2011) *Nanotribology and Nanomechanics II*. https://doi.org/10.1007/978-3-642-15263-4.

(7) Luo, T.; Lloyd, J. R. (2008) Ab Initio Molecular Dynamics Study of Nanoscale Thermal Energy Transport. *J. Heat Transfer 130* (12), 1–7. https://doi.org/10.1115/1.2976562.

(8) Martinez, N. (2009) Wettability of Silicon, Silicon Dioxide, and Organosilicate Glass. *Master Thesis*, *University*, 120.

(9) Ramos-Alvarado, B.; Kumar, S.; Peterson, G. P. (2016) On the Wettability Transparency of Graphene-Coated Silicon Surfaces. *J. Chem. Phys. 144* (1). https://doi.org/10.1063/1.4938499.

(10) Nakajima, A.; Hashimoto, K.; Watanabe, T.; Takai, K.; Yamauchi, G.; Fujishima, A. (2000) Transparent Superhydrophobic Thin Films with Self-Cleaning Properties. *Langmuir 16* (17), 7044–7047. https://doi.org/10.1021/la000155k.

(11) Barisik, M.; Beskok, A. (2013) Wetting Characterisation of Silicon (1,0,0) Surface. *Mol. Simul. 39* (9), 700–709. https://doi.org/10.1080/08927022.2012.758854.

(12) III. An Essay on the Cohesion of Fluids. (1805) *Philos. Trans. R. Soc. London*. https://doi.org/10.1098/rstl.1805.0005.

(13) Brinkmann, M.; Kierfeld, J.; Lipowsky, R. (2004) A General Stability Criterion for Droplets on Structured Substrates. *J. Phys. A. Math. Gen. 37* (48), 11547–11573. https://doi.org/10.1088/0305-4470/37/48/003.

(14) Rafiee, J.; Mi, X.; Gullapalli, H.; Thomas, A. V.; Yavari, F.; Shi, Y.; Ajayan, P. M.; Koratkar, N. A. (2012) Wetting Transparency of Graphene. *Nat. Mater.* https://doi.org/10.1038/nmat3228.

(15) Raj, R.; Maroo, S. C.; Wang, E. N. (2013) Wettability of Graphene. *Nano Lett.* https://doi.org/10.1021/nl304647t.

(16) Noginov, M. A.; Barnakov, Y. A.; Liberman, V.; Prayakarao, S.; Bonner, C. E.; Narimanov, E. E. (2016) Long-Range Wetting Transparency on Top of Layered Metal-Dielectric Substrates. *Sci. Rep.* https://doi.org/10.1038/srep27834.

(17) Chow, P. K.; Singh, E.; Viana, B. C.; Gao, J.; Luo, J.; Li, J.; Lin, Z.; Elías, A. L.; Shi, Y.; Wang, Z.; et al. (2015) Wetting of Mono and Few-Layered WS2 and MoS2 Films Supported on Si/SiO2 Substrates. *ACS Nano*. https://doi.org/10.1021/nn5072073.

(18) Dorrer, C.; Rühe, J. (2008) Wetting of Silicon Nanograss: From Superhydrophilic to Superhydrophobic Surfaces. *Adv. Mater.* https://doi.org/10.1002/adma.200701140.

(19) Gaur, A. P. S.; Sahoo, S.; Ahmadi, M.; Dash, S. P.; Guinel, M. J. F.; Katiyar, R. S. (2014) Surface Energy Engineering for Tunable Wettability through Controlled Synthesis of MoS2. *Nano Lett.* https://doi.org/10.1021/nl501106v.

(20) Ramos-Alvarado, B.; Kumar, S.; Peterson, G. P. (2015) Wettability of Graphitic-Carbon and Silicon Surfaces: MD Modeling and Theoretical Analysis. *J. Chem. Phys.* https://doi.org/10.1063/1.4927083.

(21) Shen, P.; Fujii, H.; Matsumoto, T.; Nogi, K. (2005) Surface Orientation and Wetting Phenomena in Si/α-Alumina System at 1723 K. *J. Am. Ceram. Soc.* https://doi.org/10.1111/j.1551-2916.2005.00180.x.

(22) Grzelak, E. M.; Shen, V. K.; Errington, J. R. (2010) Molecular Simulation Study of Anisotropic Wetting. *Langmuir*. https://doi.org/10.1021/la9046897.

(23) Wu, J. M.; Zhao, J. (2013) A Review of Nanofluid Heat Transfer and Critical Heat Flux Enhancement - Research Gap to Engineering Application. *Progress in*

Nuclear Energy. https://doi.org/10.1016/j.pnucene.2013.03.009.

(24) Mohammed, H. A.; Bhaskaran, G.; Shuaib, N. H.; Saidur, R. (2011) Heat Transfer and Fluid Flow Characteristics in Microchannels Heat Exchanger Using Nanofluids: A Review. *Renewable and Sustainable Energy Reviews*. https://doi.org/10.1016/j.rser.2010.11.031.

(25) Saidur, R.; Leong, K. Y.; Mohammed, H. A. (2011) A Review on Applications and Challenges of Nanofluids. *Renewable and Sustainable Energy Reviews*. https://doi.org/10.1016/j.rser.2010.11.035.

(26) Wang, X. Q.; Mujumdar, A. S. (2008) A Review on Nanofluids - Part II: Experiments and Applications. *Brazilian Journal of Chemical Engineering*. https://doi.org/10.1590/S0104-66322008000400002.

(27) Wen, D.; Ding, Y. (2004) Effective Thermal Conductivity of Aqueous Suspensions of Carbon Nanotubes (Carbon Nanotube Nanofluids). *J. Thermophys. Heat Transf. 18* (4), 481–485. https://doi.org/10.2514/1.9934.

(28) Wang, B. X.; Zhou, L. P.; Peng, X. F. (2003) A Fractal Model for Predicting the Effective Thermal Conductivity of Liquid with Suspension of Nanoparticles. *Int. J. Heat Mass Transf. 46* (14), 2665–2672. https://doi.org/10.1016/S0017-9310(03)00016-4.

(29) Xuan, Y.; Li, Q. (2000) Heat Transfer Enhancement of Nanofluids. *Int. J. Heat Fluid Flow. 21* (1), 58–64. https://doi.org/10.1016/S0142-727X(99)00067-3.

(30) St-Gelais, R.; Guha, B.; Zhu, L.; Fan, S.; Lipson, M. (2014) Demonstration of Strong Near-Field Radiative Heat Transfer between Integrated Nanostructures. *Nano Lett.* https://doi.org/10.1021/nl503236k.

(31) Rebay, M.; Kabar, Y.; Kakaç, S. (2016) Microscale and Nanoscale Heat Transfer: Analysis, Design, and Application. *CRC Press*. https://doi.org/doi:10.1201/b19261-12.

(32) Vo, T. Q.; Kim, B. H. (2015) Interface Thermal Resistance between Liquid Water and Various Metallic Surfaces. *Int. J. Precis. Eng. Manuf.* https://doi.org/10.1007/s12541-015-0176-0.

(33) Xie, J. F.; Sazhin, S. S.; Cao, B. Y. (2011) Molecular Dynamics Study of the Processes in the Vicinity of the N-Dodecane Vapour/Liquid Interface. *Phys. Fluids. 23* (11), 1–12. https://doi.org/10.1063/1.3662004.

(34) Hopkins, P. E.; Phinney, L. M.; Serrano, J. R.; Beechem, T. E. (2010) Effects of

Surface Roughness and Oxide Layer on the Thermal Boundary Conductance at Aluminum/Silicon Interfaces. *Phys. Rev. B - Condens. Matter Mater. Phys.* https://doi.org/10.1103/PhysRevB.82.085307.

(35) Kapitza, P. L. (1941) Heat Transfer and Superfluidity of Helium II. *Phys. Rev.* https://doi.org/10.1103/PhysRev.60.354.

(36) Ge, Z.; Cahill, D. G.; Braun, P. V. (2006) Thermal Conductance of Hydrophilic and Hydrophobic Interfaces. *Phys. Rev. Lett.* https://doi.org/10.1103/PhysRevLett.96.186101.

(37) Schmidt, A. J.; Alper, J. D.; Chiesa, M.; Chen, G.; Das, S. K.; Hamad-Schifferli, K. (2008) Probing the Gold Nanorod-Ligand-Solvent Interface by Plasmonic Absorption and Thermal Decay. *J. Phys. Chem. C*. https://doi.org/10.1021/jp8051888.

(38) Berber, S.; Kwon, Y. K.; Tománek, D. (2000) Unusually High Thermal Conductivity of Carbon Nanotubes. *Phys. Rev. Lett.* https://doi.org/10.1103/PhysRevLett.84.4613.

(39) Pollack, G. L. (1969) Kapitza Resistance. *Rev. Mod. Phys.* https://doi.org/10.1103/RevModPhys.41.48.

(40) Swartz, E. T.; Pohl, R. O. (1989) Thermal Boundary Resistance. *Rev. Mod. Phys.* https://doi.org/10.1103/RevModPhys.61.605.

(41) Arima, T.; Yamasaki, S.; Idemitsu, K.; Inagaki, Y. (2008) Equilibrium and Nonequilibrium Molecular Dynamics Simulations of Heat Conduction in Uranium Oxide and Mixed Uranium-Plutonium Oxide. *J. Nucl. Mater.* https://doi.org/10.1016/j.jnucmat.2008.02.067.

(42) Yenigun, O.; Barisik, M. (2019) Effect of Nano-Film Thickness on Thermal Resistance at Water/Silicon Interface. *Int. J. Heat Mass Transf.* https://doi.org/10.1016/j.ijheatmasstransfer.2019.01.075.

(43) Pham, A. T.; Barisik, M.; Kim, B. (2014) Molecular Dynamics Simulations of Kapitza Length for Argon-Silicon and Water-Silicon Interfaces. *Int. J. Precis. Eng. Manuf.* https://doi.org/10.1007/s12541-014-0341-x.

(44) Kim, B. (2012) Thermal Resistance at a Liquid-Solid Interface Dependent on the Ratio of Thermal Oscillation Frequencies. *Chem. Phys. Lett.* https://doi.org/10.1016/j.cplett.2012.10.022.

(45) WuZhi-Kin, Hui; Peng-Fei, He; Ying, D. A.-H. (2014) Molecular Dynamics

Simulation of the Thermal Conductivity of Silicon Functionalized Graphene. *Acta Phys. Sin. 63* (7), 07401.

(46) Kosmulski, M.; Eriksson, P.; Brancewicz, C.; Rosenholm, J. B. (2000) Zeta Potentials of Monodispersed, Spherical Silica Particles in Mixed Solvents as a Function of Cesium Chloride Concentration. *Colloids Surfaces A Physicochem. Eng. Asp.* https://doi.org/10.1016/S0927-7757(99)00027-8.

(47) Sidorova, M. P.; Ermakova, L. E.; Kotel'nikova, N. E.; Kudina, N. P. (2001) Electrosurface Properties of Microcrystalline Cellulose of Different Origin in 1 : 1 Electrolyte Solutions. *Colloid J.* https://doi.org/10.1023/A:1009406711746.

(48) Bogdanova, N. F.; Klebanov, A. V.; Ermakova, L. E.; Sidorova, M. P. (2002) Electrosurface Characteristics of (Hydr)Oxides and Oxide Nanostructures in 1 : 1 Electrolyte Solutions. 3. Calculation of the Electrical Double Layer Parameters for Boehmite, Goethite, and Silicon Oxide According to Adsorption and Electrokinetic Data. *Colloid J.* https://doi.org/10.1023/A:1016865916073.

(49) Ariza, M. J.; Caas, A.; Benavente, J. (2001) Electrokinetic and Electrochemical Characterizations of Porous Membranes. *Colloids Surfaces A Physicochem. Eng. Asp.* https://doi.org/10.1016/S0927-7757(01)00587-8.

(50) Underwood, T. R.; Greenwell, H. C. (2018) The Water-Alkane Interface at Various NaCl Salt Concentrations: A Molecular Dynamics Study of the Readily Available Force Fields. *Sci. Rep.* https://doi.org/10.1038/s41598-017-18633-y.

(51) Chowdhuri, S.; Chandra, A. (2001) Molecular Dynamics Simulations of Aqueous NaCl and KCl Solutions: Effects of Ion Concentration on the Single-Particle, Pair, and Collective Dynamical Properties of Ions and Water Molecules. *J. Chem. Phys.* https://doi.org/10.1063/1.1387447.

(52) Ravikumar, B.; Mynam, M.; Rai, B. (2018) Effect of Salt Concentration on Properties of Lithium Ion Battery Electrolytes: A Molecular Dynamics Study. *J. Phys. Chem. C.* https://doi.org/10.1021/acs.jpcc.8b02072.

(53) Wheeler, D. R.; Newman, J. (2004) Molecular Dynamics Simulations of Multicomponent Diffusion. 1. Equilibrium Method. *J. Phys. Chem. B.* https://doi.org/10.1021/jp047850b.

(54) Li, Z.; Smith, G. D.; Bedrov, D. (2012) Li+ Solvation and Transport Properties in Ionic Liquid/Lithium Salt Mixtures: A Molecular Dynamics Simulation Study. *J. Phys. Chem. B.* https://doi.org/10.1021/jp3052246.

(55) Taghipoor, M.; Bertsch, A.; Renaud, P. (2015) Temperature Sensitivity of Nanochannel Electrical Conductance. *ACS Nano*. https://doi.org/10.1021/acsnano.5b01196.

(56) CHIDSEY, C. E. D. (1991) Free Energy and Temperature Dependence of Electron Transfer at the Metal-Electrolyte Interface. *Science (80-.).* https://doi.org/10.1126/science.251.4996.919.

(57) Lowe, B. M.; Skylaris, C. K.; Green, N. G.; Shibuta, Y.; Sakata, T. (2018) Calculation of Surface Potentials at the Silica-Water Interface Using Molecular Dynamics: Challenges and Opportunities. In *Japanese Journal of Applied Physics*; https://doi.org/10.7567/JJAP.57.04FM02.

(58) Xu, D.; Li, D.; Leng, Y.; Chen, Y. (2007) Molecular Dynamics Simulations of Ion Distribution in Nanochannels. *Mol. Simul.* https://doi.org/10.1080/08927020701528532.

(59) Brown, M. A.; Goel, A.; Abbas, Z. (2016) Effect of Electrolyte Concentration on the Stern Layer Thickness at a Charged Interface. *Angew. Chemie - Int. Ed.* https://doi.org/10.1002/anie.201512025.

(60) Barisik, M.; Atalay, S.; Beskok, A.; Qian, S. (2014) Size Dependent Surface Charge Properties of Silica Nanoparticles. *J. Phys. Chem. C*. https://doi.org/10.1021/jp410536n.

(61) Dishon, M.; Zohar, O.; Sivan, U. (2009) From Repulsion to Attraction and Back to Repulsion: The Effect of NaCl, KCl, and CsCl on the Force between Silica Surfaces in Aqueous Solution. *Langmuir*. https://doi.org/10.1021/la803022b.

(62) Lee, D.; Kim, J. W.; Kim, B. G. (2006) A New Parameter to Control Heat Transport in Nanofluids: Surface Charge State of the Particle in Suspension. *J. Phys. Chem. B*. https://doi.org/10.1021/jp057225m.

(63) Xian-Ju, W.; Xin-Fang, L. (2009) Influence of PH on Nanofluids' Viscosity and Thermal Conductivity. *Chinese Phys. Lett.* https://doi.org/10.1088/0256-307x/26/5/056601.

(64) Yenigun, O.; Barisik, M. (2019) Electric Field Controlled Heat Transfer Through Silicon and Nano-Confined Water. *Nanoscale Microscale Thermophys. Eng.* https://doi.org/10.1080/15567265.2019.1628136.

(65) Azari, M.; Sadeghi, A.; Chakraborty, S. (2019) Graetz Problem for Combined Pressure-Driven and Electroosmotic Flow in Microchannels with Distributed Wall

Heat Flux. *Int. J. Heat Mass Transf.* https://doi.org/10.1016/j.ijheatmasstransfer.2018.08.106.

(66) Haile, J. M.; Johnston, I.; Mallinckrodt, A. J.; McKay, S. (1993) Molecular Dynamics Simulation: Elementary Methods. *Comput. Phys.* https://doi.org/10.1063/1.4823234.

(67) Richardi, J.; Fries, P. H.; Fischer, R.; Krienke, R. H. (1998) Liquid Acetone and Chloroform: A Comparison between Monte Carlo Simulation, Molecular Ornstein-Zernike Theory, and Site-Site Ornstein-Zernike Theory. *Mol. Phys.* https://doi.org/10.1080/00268979809482279.

(68) Skipper, N. T.; Sposito, G.; Chang, F. R. C. (1995) Monte Carlo Simulation of Interlayer Molecular Structure in Swelling Clay Minerals. 2. Monolayer Hydrates. *Clays Clay Miner.* https://doi.org/10.1346/CCMN.1995.0430304.

(69) Wang, A.; Modest, M. F.; Haworth, D. C.; Wang, L. (2008) Monte Carlo Simulation of Radiative Heat Transfer and Turbulence Interactions in Methane/Air Jet Flames. *J. Quant. Spectrosc. Radiat. Transf.* https://doi.org/10.1016/j.jqsrt.2007.08.030.

(70) Alder, B. J.; Wainwright, T. E. (1957) Phase Transition for a Hard Sphere System. *The Journal of Chemical Physics*. https://doi.org/10.1063/1.1743957.

(71) Rahman, A. (1964) Correlations in the Motion of Atoms in Liquid Argon. *Phys. Rev.* https://doi.org/10.1103/PhysRev.136.A405.

(72) Verlet, L. (1967) Computer "Experiments" on Classical Fluids. I. Thermodynamical Properties of Lennard-Jones Molecules. *Phys. Rev.* https://doi.org/10.1103/PhysRev.159.98.

(73) Stillinger, F. H.; Rahman, A. (1974) Improved Simulation of Liquid Water by Molecular Dynamics. *J. Chem. Phys. 60* (4), 1545–1557. https://doi.org/10.1063/1.1681229.

(74) Woodcock, L. V.; Angell, C. A.; Cheeseman, P. (1976) Molecular Dynamics Studies of the Vitreous State: Simple Ionic Systems and Silica. *J. Chem. Phys. 65* (4), 1565–1577. https://doi.org/10.1063/1.433213.

(75) McCammon, J. A.; Gelin, B. R.; Karplus, M. (1977) Dynamics of Folded Proteins. *Nature*. https://doi.org/10.1038/267585a0.

(76) Andersen, H. C. (1980) Molecular Dynamics Simulations at Constant Pressure and/or Temperature. *J. Chem. Phys. 72* (4), 2384–2393.

https://doi.org/10.1063/1.439486.

(77) Parrinello, M.; Rahman, A. (1980) Crystal Structure and Pair Potentials: A Molecular-Dynamics Study. *Phys. Rev. Lett.* https://doi.org/10.1103/PhysRevLett.45.1196.

(78) Car, R.; Parrinello, M. (1985) Unified Approach for Molecular Dynamics and Density-Functional Theory. *Phys. Rev. Lett.* https://doi.org/10.1103/PhysRevLett.55.2471.

(79) Weber, T. A.; Stillinger, F. H. (1993) Melting of Square Crystals in Two Dimensions. *Phys. Rev. E*. https://doi.org/10.1103/PhysRevE.48.4351.

(80) Vashishta, P.; Kalia, R. K.; Rino, J. P.; Ebbsjö, I. (1990) Interaction Potential for SiO2: A Molecular-Dynamics Study of Structural Correlations. *Phys. Rev. B. 41* (17), 12197–12209. https://doi.org/10.1103/PhysRevB.41.12197.

(81) Ciccotti, G.; Ferrario, M.; Hynes, J. T.; Kapral, R. (1990) Dynamics of Ion Pair Interconversion in a Polar Solvent. *J. Chem. Phys. 93* (10), 7137–7147. https://doi.org/10.1063/1.459437.

(82) Honeycutt, J. D.; Andersen, H. C. (1987) Molecular Dynamics Study of Melting and Freezing of Small Lennard-Jones Clusters. *J. Phys. Chem.* https://doi.org/10.1021/j100303a014.

(83) Tan, P.; Feng, Z.; Zhang, L.; Hou, T.; Li, Y. (2015) The Mechanism of Proton Translocation in Respiratory Complex I from Molecular Dynamics. *J. Recept. Signal Transduct.* https://doi.org/10.3109/10799893.2014.942464.

(84) Theory of Molecular Dynamics Simulations https://www.ch.embnet.org/MD_tutorial/pages/MD.Part1.html.

(85) Jones, J. E. (1924) On the Determination of Molecular Fields. II. From the Equation of State of a Gas. *Proc. R. Soc. A Math. Phys. Eng. Sci. 106* (738), 463–477. https://doi.org/10.1098/rspa.1924.0082.

(86) Plimpton, S.; Pollock, R.; Stevens, M. J. (1997) Particle Mesh Ewald and RRESPA for Parallel Molecular Dynamics Simulations. *Proc. Eighth Siam Conf. Parallel Process. Sci. Comput.* 1–13. https://doi.org/10.1.1.41.5174.

(87) Allen, M. P.; Tildesley, D. J.; Banavar, J. R. (1989) Computer Simulation of Liquids . *Phys. Today*. https://doi.org/10.1063/1.2810937.

(88) Jorgensen, W. L.; Chandrasekhar, J.; Madura, J. D.; Impey, R. W.; Klein, M. L. (1983) Comparison of Simple Potential Functions for Simulating Liquid Water. *J.*

Chem. Phys. 79 (2), 926–935. https://doi.org/10.1063/1.445869.

(89) Berendsen, H. J. C.; Grigera, J. R.; Straatsma, T. P. (1987) The Missing Term in Effective Pair Potentials. *J. Phys. Chem. 91* (24), 6269–6271. https://doi.org/10.1021/j100308a038.

(90) Van Der Spoel, D.; Van Maaren, P. J.; Berendsen, H. J. C. (1998) A Systematic Study of Water Models for Molecular Simulation: Derivation of Water Models Optimized for Use with a Reaction Field. *J. Chem. Phys. 108* (24), 10220–10230. https://doi.org/10.1063/1.476482.

(91) Miyamoto, S.; Kollman, P. A. (1992) Settle: An Analytical Version of the SHAKE and RATTLE Algorithm for Rigid Water Models. *J. Comput. Chem. 13* (8), 952–962. https://doi.org/10.1002/jcc.540130805.

(92) Ryckaert, J. P.; Ciccotti, G.; Berendsen, H. J. C. (1977) Numerical Integration of the Cartesian Equations of Motion of a System with Constraints: Molecular Dynamics of n-Alkanes. *J. Comput. Phys. 23* (3), 327–341. https://doi.org/10.1016/0021-9991(77)90098-5.

(93) Kräutler, V.; Van Gunsteren, W. F.; Hünenberger, P. H. (2001) A Fast SHAKE Algorithm to Solve Distance Constraint Equations for Small Molecules in Molecular Dynamics Simulations. *J. Comput. Chem. 22* (5), 501–508. https://doi.org/10.1002/1096-987X(20010415)22:5<501::AID-JCC1021>3.0.CO;2-V.

(94) Tao, P.; Wu, X.; Brooks, B. R. (2012) Maintain Rigid Structures in Verlet Based Cartesian Molecular Dynamics Simulations. *J. Chem. Phys. 137* (13). https://doi.org/10.1063/1.4756796.

(95) Hess, B.; Bekker, H.; Berendsen, H. J. C.; Fraaije, J. G. E. M. (1997) LINCS: A Linear Constraint Solver for Molecular Simulations. *J. Comput. Chem. 18* (12), 1463–1472. https://doi.org/10.1002/(SICI)1096-987X(199709)18:12<1463::AID-JCC4>3.0.CO;2-H.

(96) Pronk, S.; Páll, S.; Schulz, R.; Larsson, P.; Bjelkmar, P.; Apostolov, R.; Shirts, M. R.; Smith, J. C.; Kasson, P. M.; Van Der Spoel, D.; et al. (2013) GROMACS 4.5: A High-Throughput and Highly Parallel Open Source Molecular Simulation Toolkit. *Bioinformatics. 29* (7), 845–854. https://doi.org/10.1093/bioinformatics/btt055.

(97) Brooks, B. R.; Bruccoleri, R. E.; Olafson, B. D.; States, D. J.; Swaminathan, S.;

Karplus, M. (1983) CHARMM: A Program for Macromolecular Energy, Minimization, and Dynamics Calculations. *J. Comput. Chem. 4* (2), 187–217. https://doi.org/10.1002/jcc.540040211.

(98) Phillips, J. C.; Braun, R.; Wang, W.; Gumbart, J.; Tajkhorshid, E.; Villa, E.; Chipot, C.; Skeel, R. D.; Kalé, L.; Schulten, K. (2005) Scalable Molecular Dynamics with NAMD. *J. Comput. Chem. 26* (16), 1781–1802. https://doi.org/10.1002/jcc.20289.

(99) Plimpton, S. (1995) Fast Parallel Algorithms for Short-Range Molecular Dynamics. *Journal of Computational Physics*. pp 1–19. https://doi.org/10.1006/jcph.1995.1039.

(100) Leenaerts, O.; Sahin, H.; Partoens, B.; Peeters, F. M. (2013) First-Principles Investigation of B- and N-Doped Fluorographene. *Phys. Rev. B - Condens. Matter Mater. Phys. 88* (3), 1–5. https://doi.org/10.1103/PhysRevB.88.035434.

(101) Capar, M. I.; Nar, A.; Ferrarini, A.; Frezza, E.; Greco, C.; Zakharov, A. V.; Vakulenko, A. A. (2013) Molecular Structure and Elastic Properties of Thermotropic Liquid Crystals: Integrated Molecular Dynamics - Statistical Mechanical Theory vs Molecular Field Approach. *J. Chem. Phys. 138* (11). https://doi.org/10.1063/1.4794920.

(102) Erlanger, B. F.; Chen, B. X.; Zhu, M.; Brus, L. (2001) Binding of an Anti-Fullerene IgG Monoclonal Antibody to Single Wall Carbon Nanotubes. *Nano Lett. 1* (9), 465–467. https://doi.org/10.1021/nl015570r.

(103) Reisch, A.; Voegel, J. C.; Gonthier, E.; Decher, G.; Senger, B.; Schaaf, P.; Mésini, P. J. (2009) Polyelectrolyte Multilayers Capped with Polyelectrolytes Bearing Phosphorylcholine and Triethylene Glycol Groups: Parameters Influencing Antifouling Properties. *Langmuir*. https://doi.org/10.1021/la8037846.

(104) Ambrosia, M. S.; Ha, M. Y.; Balachandar, S. (2013) The Effect of Pillar Surface Fraction and Pillar Height on Contact Angles Using Molecular Dynamics. *Appl. Surf. Sci.* https://doi.org/10.1016/j.apsusc.2013.05.104.

(105) Jabbarzadeh, A. (2013) Effect of Nano-Patterning on Oleophobic Properties of a Surface. *Soft Matter*. https://doi.org/10.1039/c3sm52207e.

(106) Wei, N.; Lv, C.; Xu, Z. (2014) Wetting of Graphene Oxide: A Molecular Dynamics Study. *Langmuir*. https://doi.org/10.1021/la500513x.

(107) Fan, C. F.; Cağin, T. (1995) Wetting of Crystalline Polymer Surfaces: A Molecular

Dynamics Simulation. *J. Chem. Phys.* https://doi.org/10.1063/1.470016.

(108) Fu, T.; Wu, N.; Lu, C.; Wang, J.; Wang, Q. (2019) Effect of Nanostructure on Wettability on Copper Surface: A Molecular Dynamic Study. *Mol. Simul.* https://doi.org/10.1080/08927022.2018.1526378.

(109) Park, J. H.; Aluru, N. R. (2009) Temperature-Dependent Wettability on a Titanium Dioxide Surface. *Mol. Simul. 35* (1–2), 31–37. https://doi.org/10.1080/08927020802398884.

(110) Yen, T. H. (2011) Wetting Characteristics of Nanoscale Water Droplet on Silicon Substrates with Effects of Surface Morphology. *Mol. Simul. 37* (9), 766–778. https://doi.org/10.1080/08927022.2010.547855.

(111) Zhong, W. W.; Huang, Y. F.; Gan, D.; Xu, J. Y.; Li, H.; Wang, G.; Meng, S.; Chen, X. L. (2016) Wetting Behavior of Water on Silicon Carbide Polar Surfaces. *Phys. Chem. Chem. Phys.* https://doi.org/10.1039/c6cp04686j.

(112) Zambrano, H. A.; Walther, J. H.; Jaffe, R. L. (2014) Molecular Dynamics Simulations of Water on a Hydrophilic Silica Surface at High Air Pressures. *J. Mol. Liq.* https://doi.org/10.1016/j.molliq.2014.06.003.

(113) Baski, A. A.; Erwin, S. C.; Whitman, L. J. (1997) The Structure of Silicon Surfaces from (001) to (111). *Surf. Sci. 392* (1–3), 69–85. https://doi.org/10.1016/S0039-6028(97)00499-8.

(114) Ramos-Alvarado, B.; Kumar, S. (2017) Spectral Analysis of the Heat Flow Across Crystalline and Amorphous Si-Water Interfaces. *J. Phys. Chem. C*. https://doi.org/10.1021/acs.jpcc.7b01689.

(115) Tersoff, J. (1988) New Empirical Approach for the Structure and Energy of Covalent Systems. *Phys. Rev. B*. https://doi.org/10.1103/PhysRevB.37.6991.

(116) Batchelor, G. K. (2000) *An Introduction to Fluid Dynamics*. https://doi.org/10.1017/cbo9780511800955.

(117) Isaiev, M.; Burian, S.; Bulavin, L.; Gradeck, M.; Lemoine, F.; Termentzidis, K. (2016) Efficient Tuning of Potential Parameters for Liquid–Solid Interactions. *Mol. Simul. 42* (11), 910–915. https://doi.org/10.1080/08927022.2015.1105372.

(118) Barisik, M.; Beskok, A. (2011) Equilibrium Molecular Dynamics Studies on Nanoscale-Confined Fluids. *Microfluid. Nanofluidics*. https://doi.org/10.1007/s10404-011-0794-5.

(119) Fujii, K.; Waseda, A.; Kuramoto, N. (2001) Development of a Silicon Density

Standard and Precision Density Measurements of Solid Materials by Hydrostatic Weighing. *Meas. Sci. Technol.* https://doi.org/10.1088/0957-0233/12/12/302.

(120) Ma, P. W.; Liu, W. C.; Woo, C. H.; Dudarev, S. L. (2007) Large-Scale Molecular Dynamics Simulation of Magnetic Properties of Amorphous Iron under Pressure. *J. Appl. Phys.* https://doi.org/10.1063/1.2715753.

(121) Horbach, J. (2008) Molecular Dynamics Computer Simulation of Amorphous Silica under High Pressure. In *Journal of Physics Condensed Matter*. https://doi.org/10.1088/0953-8984/20/24/244118.

(122) Kluge, M. D.; Ray, J. R.; Rahman, A. (1987) Amorphous-Silicon Formation by Rapid Quenching: A Molecular-Dynamics Study. *Phys. Rev. B*. https://doi.org/10.1103/PhysRevB.36.4234.

(123) Ozcelik, H. G.; Ozdemir, A. C.; Kim, B.; Barisik, M. (2020) Wetting of Single Crystalline and Amorphous Silicon Surfaces: Effective Range of Intermolecular Forces for Wetting. *Mol. Simul.* https://doi.org/10.1080/08927022.2019.1690145.

(124) Kim, K. (2010) From the Future Si Technology Perspective: Challenges and Opportunities. In *Technical Digest - International Electron Devices Meeting, IEDM*. https://doi.org/10.1109/IEDM.2010.5703274.

(125) Ruiz, F.; Sun, W. D.; Pollak, F. H.; Venkatraman, C. (1998) Determination of the Thermal Conductivity of Diamond-like Nanocomposite Films Using a Scanning Thermal Microscope. *Appl. Phys. Lett.* https://doi.org/10.1063/1.122287.

(126) Mandelis, A. (1991) Photothermal Applications to the Thermal Analysis of Solids. *Journal of Thermal Analysis*. https://doi.org/10.1007/BF01932803.

(127) Esfarjani, K.; Chen, G.; Stokes, H. T. (2011) Heat Transport in Silicon from First-Principles Calculations. *Phys. Rev. B - Condens. Matter Mater. Phys.* https://doi.org/10.1103/PhysRevB.84.085204.

(128) Luo, T.; Lloyd, J. R. (2010) Equilibrium Molecular Dynamics Study of Lattice Thermal Conductivity/Conductance of Au-SAM-Au Junctions. *J. Heat Transfer*. https://doi.org/10.1115/1.4000047.

(129) Luo, T.; Lloyd, J. R. (2012) Enhancement of Thermal Energy Transport across Graphene/Graphite and Polymer Interfaces: A Molecular Dynamics Study. *Adv. Funct. Mater.* https://doi.org/10.1002/adfm.201103048.

(130) Daiguji, H. (2001) Molecular Dynamics Study of N-Alcohols Adsorbed on an Aqueous Electrolyte Solution. *J. Chem. Phys.* https://doi.org/10.1063/1.1381056.

(131) Kim, B. H.; Beskok, A.; Cagin, T. (2008) Molecular Dynamics Simulations of Thermal Resistance at the Liquid-Solid Interface. *J. Chem. Phys.* https://doi.org/10.1063/1.3001926.

(132) Kim, B. H.; Beskok, A.; Cagin, T. (2008) Thermal Interactions in Nanoscale Fluid Flow: Molecular Dynamics Simulations with Solid-Liquid Interfaces. *Microfluid. Nanofluidics*. https://doi.org/10.1007/s10404-008-0267-7.

(133) Shi, Z.; Barisik, M.; Beskok, A. (2012) Molecular Dynamics Modeling of Thermal Resistance at Argon-Graphite and Argon-Silver Interfaces. *Int. J. Therm. Sci*. https://doi.org/10.1016/j.ijthermalsci.2012.04.009.

(134) Pham, A.; Barisik, M.; Kim, B. (2013) Pressure Dependence of Kapitza Resistance at Gold/Water and Silicon/Water Interfaces. *J. Chem. Phys.* https://doi.org/10.1063/1.4851395.

(135) Barisik, M.; Beskok, A. (2014) Temperature Dependence of Thermal Resistance at the Water/Silicon Interface. *Int. J. Therm. Sci. 77*, 47–54. https://doi.org/10.1016/j.ijthermalsci.2013.10.012.

(136) *Zeta Potential in Colloid Science*; (1981). https://doi.org/10.1016/c2013-0-07389-6.

(137) Wang, Y.; Wang, L.; Hampton, M. A.; Nguyen, A. V. (2013) Atomic Force Microscopy Study of Forces between a Silica Sphere and an Oxidized Silicon Wafer in Aqueous Solutions of NaCl, KCl, and CsCl at Concentrations up to Saturation. *J. Phys. Chem. C*. https://doi.org/10.1021/jp3092495.

(138) Qiu, Y.; Ma, J.; Chen, Y. (2016) Ionic Behavior in Highly Concentrated Aqueous Solutions Nanoconfined between Discretely Charged Silicon Surfaces. *Langmuir*. https://doi.org/10.1021/acs.langmuir.6b01149.

(139) Paul, S.; Chandra, A. (2003) Dynamics of Water Molecules at Liquid-Vapour Interfaces of Aqueous Ionic Solutions: Effects of Ion Concentration. *Chem. Phys. Lett.* https://doi.org/10.1016/S0009-2614(03)00537-2.

(140) Ozbek, H.; Phillips, S. L. (1980) Thermal Conductivity of Aqueous Sodium Chloride Solutions from 20 to 330. Degree. CThermal Conductivity of Aqueous Sodium Chloride Solutions from 20 to 330 °C. *J. Chem. Eng. Data*. https://doi.org/10.1021/je60086a001.

(141) Rezaei, M.; Azimian, A. R.; Semiromi, D. T. (2015) The Surface Charge Density Effect on the Electro-Osmotic Flow in a Nanochannel: A Molecular Dynamics

Study. *Heat Mass Transf. und Stoffuebertragung*. https://doi.org/10.1007/s00231-014-1441-y.

(142) Jelinek, B.; Felicell, S. D.; Mlakar, P. F.; Peters, J. F. (2010) Molecular Dynamics Study of Temperature Effects on Electrokinetic Transport in Si Nanochannel. In *ASME International Mechanical Engineering Congress and Exposition, Proceedings*;. https://doi.org/10.1115/IMECE2009-11690.

(143) Farnam, Y.; Bentz, D.; Sakulich, A.; Flynn, D.; Weiss, J. (2014) Measuring Freeze and Thaw Damage in Mortars Containing Deicing Salt Using a Low-Temperature Longitudinal Guarded Comparative Calorimeter and Acoustic Emission. *Adv. Civ. Eng. Mater.* https://doi.org/10.1520/acem20130095.

(144) Patra, M.; Karttunen, M. (2004) Systematic Comparison of Force Fields for Microscopic Simulations of NaCl in Aqueous Solutions: Diffusion, Free Energy of Hydration, and Structural Properties. *J. Comput. Chem.* https://doi.org/10.1002/jcc.10417.

(145) Dove, P. M.; Craven, C. M. (2005) Surface Charge Density on Silica in Alkali and Alkaline Earth Chloride Electrolyte Solutions. *Geochim. Cosmochim. Acta*. https://doi.org/10.1016/j.gca.2005.05.006.

(146) Barisik, M.; Beskok, A. (2012) Boundary Treatment Effects on Molecular Dynamics Simulations of Interface Thermal Resistance. *J. Comput. Phys.* https://doi.org/10.1016/j.jcp.2012.07.026.

(147) Mao, Y.; Zhang, Y. (2012) Thermal Conductivity, Shear Viscosity and Specific Heat of Rigid Water Models. *Chem. Phys. Lett.* https://doi.org/10.1016/j.cplett.2012.05.044.

(148) Vo, T. Q.; Kim, B. H. (2015) Interface Thermal Resistance between Liquid Water and Various Metallic Surfaces. *Int. J. Precis. Eng. Manuf. 16* (7), 1341–1346. https://doi.org/10.1007/s12541-015-0176-0.

(149) Song, G.; Min, C. (2013) Temperature Dependence of Thermal Resistance at a Solid/Liquid Interface. *Mol. Phys.* https://doi.org/10.1080/00268976.2012.756990.